**Biogeosciences
Discussions**

Biogeosciences Discussions is the access reviewed discussion forum of *Biogeosciences*

On the application and interpretation of Keeling plots in paleo climate research – deciphering δ^{13}C of atmospheric CO$_2$ measured in ice cores

P. Köhler, J. Schmitt, and H. Fischer

Alfred Wegener Institute for Polar and Marine Research, P.O. Box 12 01 61, 27515 Bremerhaven, Germany

Correspondence to: P. Köhler (pkoehler@awi-bremerhaven.de)

Abstract

The Keeling plot analysis is an interpretation method widely used in terrestrial carbon cycle research to quantify exchange processes of carbon between terrestrial reservoirs and the atmosphere. Here, we analyse measured data sets and artificial time series of the partial pressure of atmospheric carbon dioxide (pCO$_2$) and of δ^{13}C of CO$_2$ over industrial and glacial/interglacial time scales and investigate to what extent the Keeling plot methodology can be applied to longer time scales. The artificial time series are simulation results of the global carbon cycle box model BICYCLE. Our analysis shows that features seen in pCO$_2$ and δ^{13}C during the industrial period can be interpreted with respect to the Keeling plot. However, only a maximum of approximately half of the signal can be explained by this method. The signals recorded in ice cores caused by abrupt terrestrial carbon uptake or release loose information due to air mixing in the firn before bubble enclosure and limited sampling frequency. For less abrupt changes as occurring during glacial cycles carbon uptake by the ocean cannot longer be neglected. We introduce an equation for the calculation of the effective isotopic signature of long-term changes in the carbon cycle, in which the ocean is introduced as third reservoir. This is a paleo extention of the two reservoir mass balance equations of the Keeling plot approach. Steady state analyses of changes in the terrestrial and marine biosphere lead to similar effective isotopic signatures (-8.6‰) of the carbon fluxes perturbing the atmosphere. These signatures are more positive than the δ^{13}C signals of the sources, e.g. the terrestrial carbon pools themselves (~ -25‰). In all other cases the effective isotopic signatures are larger (-8.2‰ to -0.7‰), and very often indistinguishable in the light of the uncertainties. Therefore, a back calculation from well distinct fluctuations in pCO$_2$ and δ^{13}C to identify their origin using the Keeling plot approach seems not possible.

1 Introduction

In carbon cycle research information on the origin of fluxes between different reservoirs as contained in the ratio of the stable carbon isotopes $^{13}C/^{12}C$ has become more and more important in the past decades. These isotopic signatures store information about exchange processes because differences in physical properties of atoms and molecules containing different isotopes of an element lead to isotopic fractionation.

Prominent examples in our context of global carbon cycle research are gas exchange between surface ocean and atmosphere or photosynthetic production in both the marine and the terrestrial biosphere. Here, the end member of a carbon flux associated with a given process is in general depleted in the heavier isotope. This is expressed with the fractionation factor ε of the process, which depends on various environmental parameters such as temperature or the biological species (see Zeebe and Wolf-Gladrow (2001) for more basic information on carbon isotopes in seawater).

The isotopic composition of a reservoir is usually expressed in per mil (‰) in the so-called "δ-notation" as the relative deviation from the isotope ratio of a defined standard (VPDP in the case of $\delta^{13}C$):

$$\delta^{13}C_{\text{sample}} = \left(\frac{\frac{[^{13}C]}{[^{12}C]}_{\text{sample}}}{\frac{[^{13}C]}{[^{12}C]}_{\text{standard}}} - 1 \right) \times 10^3. \tag{1}$$

The fractionation factor ε (in ‰) between carbon in sample A and in sample B (e.g. before and after some fractionation step) is related to the δ values by

$$\varepsilon_{(A-B)} = \frac{\delta^A - \delta^B}{1 + \delta^B/10^3}. \tag{2}$$

During photosynthesis the carbon taken up by marine primary producers is typically depleted by -16 to -20‰. On land, the type of metabolism determines the fractionation factor during terrestrial photosynthesis. C_3 plants inhibit a higher discrimination against

the heavy isotope ($\varepsilon=-15$ to -23‰) than plants with C_4 metabolism ($\varepsilon=-2$ to -8‰) (Mook, 1986).

One prominent interpretation technique of carbon exchange between the atmosphere and other reservoirs, e.g used in carbon flux studies in terrestrial ecosystems, is plotting the $\delta^{13}C$ signature of CO_2 as a function of the inverse of the atmospheric carbon dioxide mixing ratio ($\delta^{13}C=f(1/CO_2)$). In doing so, the intercept of a linear regression with the y-axis can under certain conditions be understood as the isotopic signature of the flux, which alters the content of carbon in the atmospheric reservoir. This approach is called "Keeling plot" after the very first usage by Charles D. Keeling about 50 years ago (Keeling, 1958, 1961). The application and interpretation of Keeling plots is widely used in terrestrial carbon research and based on some fundamental assumptions (see review of Pataki et al., 2003).

Keeling plots have also been used in paleo climate research in the past years (e.g. Smith et al., 1999; Fischer et al., 2003), but it seems that the limitations of this approach have not been adequately taken into account to allow for a meaningful interpretation. The aim of this paper therefore is to emphasise what can be learnt from Keeling plots, if applied on slow, but global processes acting on glacial/interglacial time scales, and to discuss their limitations. We emphasise what kind of information can be gained from deciphering the $\delta^{13}C$ signal measured in ice cores. For this purpose we extent the Keeling plot approach to a three reservoir system and analyse data sets and artificial time series produced by a global carbon cycle box model, from which we know which processes are operating.

2 The Keeling plot

The principle of the Keeling plot approach is based on the exchange process of carbon between two reservoirs and the conservation of mass. Let C_{new} be the mass of carbon

after the addition of carbon with mass C_{add} to an undisturbed reservoir with mass C_{old}.

$$C_{new} = C_{old} + C_{add} \tag{3}$$

With $\delta^{13}C_x$ being the carbon isotope signature of the C component x the conservation of mass thus gives us:

$$C_{new} \cdot \delta^{13}C_{new} = C_{old} \cdot \delta^{13}C_{old} + C_{add} \cdot \delta^{13}C_{add} \tag{4}$$

In combining Eqs. (3) and (4) we obtain a relationship between $\delta^{13}C_{new}$ and C_{new}:

$$\delta^{13}C_{new} = C_{old} \cdot (\delta^{13}C_{old} - \delta^{13}C_{add}) \cdot \frac{1}{C_{new}} + \delta^{13}C_{add} \tag{5}$$

Thus, the y-intercept y_0 of the linear regression function of Eq. (5), which describes $\delta^{13}C_{new}$ as a function of the inverse of the carbon content ($1/C_{new}$), gives us the isotopic ratio $\delta^{13}C_{add}$ of the carbon added to the reservoir.

There are two basic assumptions underlying the Keeling plot method: (1) The system consists of two reservoirs only. (2) The isotopic ratio of the added reservoir does not change during the time of observation. Both assumptions are only rarely fulfilled. Furthermore, there are arguments about which linear regression model should be used if one assumes measurement errors in both variables (for details see Pataki et al., 2003). The methodological aspects concerning the choice of a regression model are not the subject of our investigations here.

The Keeling plot approach was used in the past to interpret various different subsystems of the global carbon cycle. Keeling (1958, 1961) first used it to identify the contribution of terrestrial plants to the background isotopic ratio of CO_2 in a rural area near the Pacific coast of North America. Later, the component of the terrestrial biosphere in the seasonal cycle of CO_2 over Switzerland (Friedli et al., 1986; Sturm et al., 2005) and Eurasia (Levin et al., 2002) was investigated with the Keeling plot. The approach was widely used in terrestrial ecosystem research to identify respiration fluxes (e.g. Flanagan and Ehleringer, 1998; Yakir and Sternberg, 2000; Bowling et al., 2001;

Pataki et al., 2003; Hemming et al., 2005). It was used in paleo climate research within the last years to disentangle the processes explaining the subtle changes in CO_2 during the relatively stable LGM and the Holocene as well as the approximately 80 ppmv increase from the Last Glacial Maximum (LGM) to the Early Holocene (Smith et al., 1999; Fischer et al., 2003; Eyer, 2004).

3 Global CO_2 and $\delta^{13}C$ times series of different temporal resolution

It has been shown (Fischer et al., 2003), that the seasonal amplitude of CO_2 and $\delta^{13}C$ during the last decades, the anthropogenic rise in CO_2 and the corresponding decrease in its $\delta^{13}C$ signal since 1750 AD, and the glacial/interglacial variation in these two records exhibit significant different behaviour if analysed with the Keeling plot approach. Data sets showing these dynamics on the three different temporal scales are compiled in Fig. 1. The seasonal signal is measured from 1982 to 2002 AD at Point Barrow, Alaska (Keeling and Whorf, 2005; Keeling et al., 2005). For the anthropogenic variation during the last millennium we use the data measured in air enclosures in the Law Dome ice core (Francey et al., 1999; Trudinger et al., 1999). Glacial/interglacial variations (1–30 kyr BP) were detected in the Taylor Dome ice core (Smith et al., 1999). For the interpretation of the seasonal signal measured at Point Barrow both data sets (CO_2, $\delta^{13}C$) need to be detrended to separate the two simultaneous occurring effects of the anthropogenic CO_2 rise and the seasonality from each other. Annual variations are then analysed as perturbations from the mean values during the first year of the measurements. The component C_{add} in Eqs. (3)–(5) reflects the exchange of carbon of an external reservoir (winter time carbon release from the terrestrial biosphere in the seasonal signal of Point Barrow and anthropogenic emissions in the case of Law Dome) with the atmospheric reservoir. The Point Barrow and Law Dome data can be approximated consistently with the typical Keeling plot linear regression function (r^2=96% in both). The y-axis intercept y_0 declines from the seasonal effects (−25‰) to the anthropogenic impact (−13‰) with the mixed signal of the untreated data at Point

Barrow in-between (−17‰) (Fig. 1b). This decline is explained by a larger oceanic carbon uptake and a smaller airborne fraction of any atmospheric disturbance in CO_2 in longer time scales (Fischer et al., 2003).

These two examples based on accurate data sets are already beyond Keelings original idea as they are no longer based on a two reservoir system and highlight the limitations of this approach. While the y-intercept of the detrended data at Point Barrow match the expectations well, the intercept found in the anthropogenic rise in Law Dome does not record the $\delta^{13}C$ signal of the carbon released by anthropogenic activity (with $\delta^{13}C$ of about −25 to −30‰) to the atmosphere anymore. The seasonal amplitude at Point Barrow can be explained with the seasonality of the terrestrial biosphere. Vegetation grows mainly in the northern hemisphere, and thus CO_2 minima occur during maximum photosynthetic carbon uptake by plants during northern summer. The seasonal fluctuation in CO_2 should therefore bear a $\delta^{13}C$ signal of the order of −25‰ which would account for fractionation during terrestrial photosynthesis (Scholze et al., 2003). This $\delta^{13}C$ signal of the seasonal cycle is seen in the detrended Point Barrow data and corresponds well with other studies (e.g. Levin et al., 2002). The anthropogenic rise seen in the Law Dome data set is the residual of the combination of fossil fuel emissions (Marland et al., 2005), land use changes (Houghton, 2003), terrestrial carbon sinks due to CO_2 fertilisation (Plattner et al., 2002), all from which the ocean carbon uptake during that time has to be subtracted. Until about 1910 AD the fossil fuel emissions were smaller than the carbon release caused by land use change (both around $0.8\,\text{PgC yr}^{-1}$). The relation changed thereafter and in the year 2000 AD fossil fuel emissions were already more than three times larger than carbon fluxes based on land use change (6.7 versus $2.1\,\text{PgC yr}^{-1}$; Fig. 2a). The cumulative release of fossil fuel carbon out-competed that from land use change only in year 1973 AD. Altogether about 465 Pg of carbon were released by anthropogenic activities during this 250 year period to the atmosphere (Fig. 2b). Without carbon uptake by the ocean and the terrestrial reservoirs this would have led to a rise in atmospheric CO_2 by more than 200 ppmv. The $\delta^{13}C$ signal of recent fossil fuel emissions in the USA is around −29 to

519

−30‰ (Blasing et al., 2004), while carbon fluxes from land use changes bear the typical $\delta^{13}C$ signal of the terrestrial biosphere (−25‰). These anthropogenic processes can by no means be deconvoluted by the Keeling plot analysis. The reason for this is that due to the gas exchange between ocean and atmosphere the basic assumption of a two reservoir system is intrinsically violated. This questions the applicability of the Keeling plot approach to carbon change studies on long time scales, where this ocean/atmosphere gas exchange becomes even more significant.

Going further back in time, the glacial/interglacial rise in CO_2 and its accompanied $\delta^{13}C$ variations as measured in the Taylor Dome ice core led to a sub-grouping of the $\delta^{13}C$−$1/CO_2$ data pairs (Smith et al., 1999) with different linear regression functions for the Last Glacial Maximum (LGM), the glacial-interglacial transition (GIG), and the Holocene (HOL) (Fig. 1b). With on average one data point every thousand years the data set is sparse. However, the y-intercepts during LGM and Holocene are similar (−9.5‰) and significantly different from that during the transition (−5.8‰). Thus, it was hypothesised that underlying processes for variations in CO_2 during the relatively stable climates of the LGM and the Holocene might have been the same and might have been mainly based on processes concerning the terrestrial biosphere (Smith et al., 1999; Fischer et al., 2003).

4   Extending the Keeling plot approach to a three reservoir system

A first estimate for the effective carbon isotopic signature in the atmosphere due to an injection of terrestrial carbon into the ocean/atmosphere system can be derived when extending the two reservoirs to a three reservoir system. Here we assume that ocean circulation remained the same and that an equilibrium between ocean and atmosphere is achieved.

We have to extend the carbon and isotopic balance according to

$$A + O = A_0 + O_0 + B \qquad\qquad (6)$$

520

and

$$A\delta^A + O\delta^O = A_0\delta_0^A + O_0\delta_0^O + B\delta^B. \tag{7}$$

where $A_0 = 600\,\text{PgC}$ and $O_0 = 38\,000\,\text{PgC}$ are the reservoir sizes of the atmosphere and ocean, respectively, before an injection of terrestrial carbon of the size B. A and O are the sizes of the atmospheric and oceanic reservoirs after the injection. The δ_0's represent the carbon isotopic signatures of the reservoirs before the injection with $\delta_0^A = -6.5‰$ and $\delta_0^O = +1.5‰$ and the δ's after the injection. The isotopic signature of the terrestrial biosphere $\delta^B = -25‰$ is assumed to be constant. Note, that during the gas exchange and the dissociation of carbonic acid in the seawater fractionation occurs (according to Eq. 2) $\varepsilon_{AO} \approx \delta_0^A - \delta_0^O \approx \delta^A - \delta^O \approx -8‰$, which is assumed to remain constant in time.

For the oceanic uptake of carbon we have to take the buffering effect of the carbonate system in seawater into account (Zeebe and Wolf-Gladrow, 2001). The ratio between the change in CO_2 concentration and the change in dissolved inorganic carbon (DIC) is described by the Revelle or buffer factor β, which is temperature, alkalinity and DIC dependent:

$$\beta := \left(\frac{d[CO_2]/[CO_2]}{d\,DIC/DIC} \right). \tag{8}$$

Any additional carbon injected into the ocean/atmosphere system will be distributed in the two reservoirs according to the ratio of the sizes before the injection, i.e.

$$\frac{A - A_0}{O - O_0} = \beta \frac{A_0}{O_0}. \tag{9}$$

Using the carbon balance in Eq. (6) we can calculate the size of the ocean and atmosphere reservoir after the injection

$$O = \frac{\beta A_0 + O_0 + B}{\beta A_0/O_0 + 1}. \tag{10}$$

The Revelle factor β in recent surface waters varies between 8 and 16 (Sabine et al., 2004). For the preindustrial setting β in the surface ocean boxes of our box model BICYCLE is on average 11.5, with 9 in equatorial waters and around 12 in the high latitudes. Note that the average Revelle factor of the surface ocean falls to 10 for the climatic conditions of the LGM.

The effective carbon signature of the isotopic change in the atmosphere $\delta^{\Delta A}$ can be estimated according to

$$\delta^{\Delta A} = \frac{A\delta^A - A_0\delta_0^A}{A - A_0}. \tag{11}$$

Using the carbon isotopic balance in Eq. (7) and replacing $\delta^O = \delta^A - \varepsilon_{AO}$ we obtain

$$\delta^{\Delta A} = \frac{\frac{A_0 + O_0 + B - O}{A_0 + O_0 + B}(A_0\delta_0^A + O_0\delta_0^O + B\delta^B + \varepsilon_{AO}O) - A_0\delta_0^A}{O_0 + B - O}. \tag{12}$$

When we insert the values for isotopic signatures and reservoir sizes given above and vary the amount of terrestrial carbon added, the isotopic fractionation during gas exchange ε_{AO} or the Revelle factor β we obtain varying effective isotopic signatures $\delta^{\Delta A}$ of the change in the atmospheric carbon reservoir as shown in Fig. 3. In a setting for the preindustrial climate conditions, $\delta^{\Delta A}$ varies nearly linear with B between $-9‰$ and $-10‰$ (Fig. 3a), reflecting the progressive lightening of the overall ocean/atmosphere system the more isotopically depleted terrestrial carbon is added. Note, that these values are similar to the ones derived by Smith et al. (1999) and Fischer et al. (2003) both for the Holocene and the LGM from Taylor Dome ice core data and which have been interpreted as indicative of terrestrial carbon reservoir changes during these periods. However, from the interpretation of other processes changing the global carbon cycle following in Sect. 5.3 it will become apparent that not only terrestrial carbon release can produce this kind of signal.

In the special case with a Revelle factor $\beta = 1$ (no carbonate buffering), and $\varepsilon_{AO} = 0‰$, (no isotopic fractionation during air/sea transfer), $\delta^{\Delta A}$ records correctly the isotopic

signature $\delta^B = -25‰$ of the terrestrial carbon release (Fig. 3b). In all other cases, both the buffering of the ocean and the isotopic fractionation during gas exchange have a significant influence on the calculated $\delta^{\Delta A}$ with the change in the Revelle factor having the strongest effect for typical ocean surface conditions.

This reveals three major findings:

1. The isotopic signature $\delta^{\Delta A}$ is dependent on the amount of carbon injected and the setting of the system described by the three reservoirs, their isotopic signatures, the fractionation factors, and the Revelle factor.

2. For realistic settings $\delta^{\Delta A}$ stays between of -8.5 and $-10‰$. The signal which can be detected is therefore much more enriched in ^{13}C than the carbon released from the terrestrial biosphere with $\delta^B = -25‰$, which was the origin of the perturbation.

3. There exists a boundary $\delta^{\Delta A}_{\delta C \to 0}$ in the effective signature of the isotopic change in atmospheric δ^{13}C which is reached if the amount of carbon released to the atmosphere converges to zero. Note, that $\delta^{\Delta A}$ is not defined for $B = 0$ PgC, because the denominator in Eq. (12) becomes zero. Perturbations in the system will only lead to variations in $\delta^{\Delta A}$ from this boundary.

Only for processes which are faster than the equilibration time of the deep ocean with the atmosphere, substantial amounts of isotopic depleted carbon stay in the atmosphere allowing for more negative effective $\delta^{\Delta A}$ values in the Keeling plot. The latter is seen e.g. for the seasonal variation in CO_2 due to the waxing and waning of the biosphere and to a smaller extent also for the input of isotopically depleted anthropogenic carbon into the atmosphere which has a typical time scale of decades to centuries.

The two reservoir system is a special case of these calculation for a three reservoir system when $\beta = 1$ and $\varepsilon_{AO} = 0‰$, i.e. when the atmosphere and the ocean can be treated as one homogeneous reservoir. The effective carbon isotopic signature $\delta^{\Delta A}$ based on our theoretical consideration as calculated in this section is comparable with the y_0 of a linear regression in a Keeling plot performed on measured or simulated data

sets. However, details in the marine carbon cycle, such as spatial variations in the Revelle factor, ocean circulation schemes and the ocean carbon pumps which introduce vertical gradients in DIC and ^{13}C in the ocean prevent us from a direct comparison of the obtained values. Nevertheless, the theoretical exercise above gives us valuable insights for the interpretation of the artificial data sets, which will be discussed in the following.

5 Artificial ρCO_2 and δ^{13}C times series

Recently, a time-dependent modelling approach gave a quantitative interpretation of the dynamics of the atmospheric carbon records over Termination I by forcing the global ocean/atmosphere/biosphere carbon cycle box model BICYCLE forward in time (Köhler et al., 2005a). They identified the impacts of different processes acting on the carbon cycle on glacial/interglacial time scales and proposed a scenario, which provides an explanation the evolution of ρCO_2, δ^{13}C, and Δ^{14}C over time. The results are in line with various other paleo climatic observations.

In the following we will reanalyse the results of Köhler et al. (2005a) by applying the Keeling plot analysis to study whether this kind of analysis applied on paleo climatic changes in atmospheric CO_2 and δ^{13}C can lead to meaningful results. Additionally, further simulations with the BICYCLE model will be performed. The advantage of using model-generated artificial time series is, that we know which processes are operating and which process-dependent isotopic fractionations influence the δ^{13}C signals of the results. We highlight how the Keeling plot approach can gain new insights from these data sets and where its limitations in paleo climatic research seem to be.

Since BICYCLE does not resolve seasonal phenomena we are unable to interpret or reconstruct the dynamics of the Point Barrow data set of the last decades. However, we are able to implement the anthropogenic impacts of the last 250 years as seen in the Law Dome ice core. After a short model description and an interpretation of this data set as a sort of ground truthing for our analysis, we dig into the glacial/interglacial

mystery of the carbon cycle and re-evaluate the Taylor Dome ice core data set.

Please note, that atmospheric scientists typically measure carbon dioxide as volume mixing ratio in parts per million and volume (ppmv) in dry air. Marine chemists and the artificial records produced by our model give carbon dioxide as partial pressure (pCO$_2$) given in units of μatm. Only in dry air and at standard pressure, they are numerically equal (Zeebe and Wolf-Gladrow, 2001).

5.1 The global carbon cycle box model BICYCLE

The box model of the global carbon cycle BICYCLE consists of an ocean module with ten homogeneous boxes in three basins (Atlantic, Southern Ocean, Indo-Pacific) and three different vertical layers (surface, intermediate, deep), a globally averaged atmospheric box and a terrestrial module with seven globally averaged compartments representing ground and tree vegetation and soil carbon with different turnover times (Fig. 4). Prognostic variables in the model are DIC, alkalinity, oxygen, phosphate and the carbon isotopes ^{13}C and ^{14}C in the ocean boxes, and carbon and its carbon isotopes in the atmosphere and terrestrial reservoirs. The net difference between sedimentation and dissolution of CaCO$_3$ is calculated from variations of the lysocline and imposes fluxes of DIC and alkalinity between deep ocean and sediment. The model is completely described in Köhler and Fischer (2004) and Köhler et al. (2005a). BICYCLE is based in its architecture on earlier box models used during the past two decades (Emanuel et al., 1984; Munhoven, 1997). It was adapted to be able to answer questions of paleo climate research with its whole parameterisation being updated.

We apply disturbances of the climate system through the use of forcing functions and paleo climate records (e.g. changes in temperature, sea level, aeolian dust input in the Southern Ocean) and prescribe changes in ocean circulation over time based on other data- and model-based studies. BICYCLE is then able to reconstruct the evolution of atmospheric pCO$_2$, δ^{13}C, and Δ^{14}C during the last glacial/interglacial transition (Köhler et al., 2005a). It was further used to simulate variations of atmospheric CO$_2$ during the last eight glacial cycles (Wolff et al., 2005; Köhler and Fischer, 2006), and to analyse

the implication of changes in the carbon cycle on atmospheric Δ^{14}C (Köhler et al., 2006[1]).

5.2 Anthropogenic emissions – ground truth of the paleo Keeling plot approach

We implement a data-based estimate of the anthropogenic emission since 1750 AD in our model as seen in Fig. 2. BICYCLE calculates pCO$_2$ depending on the dynamics of the terrestrial biosphere. In the more realistic case of an active terrestrial biosphere, implying an enhanced photosynthesis and thus carbon uptake through CO$_2$ fertilisation, pCO$_2$ at year 2000 is calculated to 351 μatm (Fig. 5c). A scenario with passive terrestrial biosphere, meaning a constant carbon storage over time, leads to 388 μatm in the same year (Fig. 5a). The annual mean in year 2000 in the atmospheric CO$_2$ data at Point Barrow is 371 ppmv, which is approximately half way between the results of the two different simulation scenarios. The scenario with passive terrestrial biosphere is easier to interpret, since we only have to consider the anthropogenic carbon flux to the atmosphere and the effect of the oceanic sink. Both scenarios will be analysed in the following.

The precise value of the δ^{13}C signature of anthropogenic carbon release is still uncertain, e.g. land use change has a δ^{13}C of −25‰ (Scholze et al., 2003), while δ^{13}C of fossil fuel emissions is around −30‰ (Blasing et al., 2004). We therefore varied the isotopic signature of the anthropogenic carbon fluxes between −20‰ and −30‰ to evaluate the importance of this signature for the simulation results. The simulated atmospheric δ^{13}C in year 2000 AD was −8.4, −9.1, −9.7‰ and −7.4, −7.9, −8.4‰ in the scenario with passive and active terrestrial biosphere and for different δ^{13}C signatures (−20‰, −25‰, −30‰), respectively (Figs. 5a, c), reflecting a larger terrestrial

---

[1]Köhler, P., Muscheler, R., and Fischer, H.: A model-based interpretation of low frequency changes in the carbon cycle during the last 120 kyr and its implications for the reconstruction of atmospheric Δ^{14}C, Geochemistry, Geophysics, Geosystems, in review, doi:10.1029/2005GC001228, 2006.

fixation of anthropogenic carbon in the active scenario. The annual average δ^{13}C measured at different globally distributed stations varied between −8.0‰ and −8.2‰ (Keeling et al., 2005).

The regression functions of the Keeling approach are still a good approximation of the artificial data sets ($r^2 \geq 94\%$, Figs. 5b, d). However, the y-axis intercept varies depending on the assumed δ^{13}C signal of the anthropogenic carbon flux and the mode of the terrestrial biosphere (active/passive) between −9.2‰ and −15.7‰, while the Law Dome data show −13.1‰ (Table 1). Note, that these numbers are significantly higher than the isotopic signature of the anthropogenic carbon added to the system. Due to the non-negligible effect of a third reservoir, the ocean, the Keeling y-axis intercept deviates from the expected flux signature derived in Sect. 4. Normalised to the δ^{13}C signal of the anthropogenic flux the y-axis intercept amounts to 52−59% (passive terrestrial biosphere) and 45−46% (active terrestrial biosphere) of the isotopic signal of the anthropogenic flux (Table 1). The difference to an ideal Keeling plot, in which the whole signal would be explained by the y-axis intercept has to be explained purely by oceanic uptake in the case of a passive terrestrial biosphere, and by a mixture of terrestrial and oceanic uptake in simulations with active terrestrial biosphere.

Natural changes in atmospheric CO_2 over the past 650 000 years as recorded in Antarctic ice core records (Petit et al., 1999; Siegenthaler et al., 2005) were always slower and smaller in amplitude than the anthropogenic impact of the last 250 years. Therefore it is conservative to assume that the oceanic uptake of a terrestrial disturbance in the past will always be greater than during the anthropogenic period. The potential of the Keeling plot approach to paleo climate research therefore seems to have an upper limit. No more than about 50% of the isotopic signature of a carbon source to the atmosphere can be explained with it. In fact, due to the longer time scales on which most processes act during glacial cycles it can be expected that much less than this upper limit can be explained by the Keeling plot approach. For steady state situations (the atmosphere and the ocean are in equilibrium) the perturbation of the carbon cycle through terrestrial carbon release with a signature of −25‰ leads to

a $\delta^{\Delta A}_{\delta C \to 0}$ of about −9‰, as shown in Sect. 4. Thus, for this situations only a fraction of 9/25=0.36 is explainable with the Keeling plot approach.

5.3 Glacial/interglacial times

Besides this upper limit of a signal interpretation due to oceanic carbon uptake in long time series two other factors make a comparison of artificial time series with long ice core data sets difficult: First, the air which is enclosed in bubbles in the ice can circulate through the firn down to the depth where bubble close off occurs ($\sim$70−100 m) before it is entrapped in the ice. The bubble close off is a slow process with individual bubbles closing at different times and depth. Accordingly the air enclosed in bubbles and in an ice sample is subject to a wide age distribution acting as an efficient low-pass filter on the atmospheric record. Therefore, all information from the gaseous components of the ice cores is averaged over a time interval of the age of the firn/ice transition zone. This time interval is depending on temperature and accumulation rates, but can roughly be estimated by the ratio of the depth of the firn/ice transition zone divided by the accumulation rate (Schwander and Stauffer, 1984). Thus, the time integral in the gas is small (<20 years) at Law Dome (Etheridge et al., 1996), varies at Taylor Dome between 150 years in the Holocene and 300 years in the LGM (Steig et al., 1998a,b), and at EPICA Dome C, at which the most recent CO_2 and δ^{13}C measurements were performed (Monnin et al., 2001; Eyer, 2004; Eyer et al., 2004; Siegenthaler et al., 2005), between 300 and 600 years (Schwander et al., 2001). Second, the CO_2 and δ^{13}C records retrieved from ice cores are never continuous records, but consist of single measurements with large, but un-regular data gaps in between. In the Taylor Dome ice core these gaps are on average approximately 1000 years wide. It will be therefore of interest to investigate if the temporal resolution in the data set will be sufficient enough to resolve information potentially retrievable through the Keeling approach.

Anthropogenic activities add carbon via land use change and fossil fuel emissions to the atmosphere, and are only subsequently absorbed by the ocean. The

causes for natural changes in atmospheric CO_2 and thus the carbon cycle during glacial/interglacial times were to a large extent located in the ocean. Thus, the causes and effects respectively their timing are in principle different. For the natural glacial/interglacial variations the carbon content of the atmosphere is determined by the surface ocean, the atmosphere is also called "slave to the ocean", while for the anthropogenic impact the opposite is the case: The carbon of the surface ocean is modified by the injection of the anthropogenic rise in atmospheric CO_2.

This situation has also consequences for the investigation of different processes causing natural changes in the carbon cycle. We concentrate in the following on the individual impacts of six important processes. We first investigate the maximum impacts possible from changes in these processes and then analyse variations of realistic amplitude. These processes are changes in terrestrial carbon storage, export production of the marine biota, ocean circulation, gas exchange rates and their variation through variable sea ice cover, and physical effects of variable sea level and ocean temperature. Please note, that in these factorial scenarios all processes can be treated un-coupled in our box model, e.g. changes in the circulation scheme will not lead to temperature variations, which might be the case in general circulation models. A summary of this single process analysis is compiled in Table 3. We end with a combined scenario proposed by Köhler et al. (2005a) which is able the reconstruct the atmospheric carbon records between 20 and 10 kyr BP. Note, that from these different scenarios only the first one (changes in terrestrial carbon storage) strictly resembles the initial idea of a Keeling plot (addition/subtraction of carbon from the atmosphere).

5.3.1 Terrestrial biosphere

There are two opposing changes in terrestrial carbon storage to be investigated: carbon uptake or carbon release. Both might happen very fast in the course of abrupt climate anomalies, such as so-called Dansgaard/Oeschger events (Dansgaard et al., 1982; Johnsen et al., 1992), during which Greenland temperatures rose and dropped by more than 15 K in a few decades during the last glacial cycle (Lang et al., 1999;

Landais et al., 2004). Terrestrial carbon storage anomalies during these events were estimated with a dynamic global vegetation model to be of the order of $50-100$ PgC (Köhler et al., 2005b). The time scales of these anomalies are of the order of centuries to millenia. We first analyse a scenario in which 10 PgC are released or taken up by the terrestrial pools within one year. This short time frame of one year was chosen to have experiments, in which the whole carbon flux is first altering the atmospheric reservoir, before oceanic uptake or release responds after year one. The amplitude of the perturbations is optimised to 10 PgC to guarantee still negligible numerical uncertainties (<0.01‰) in the calculation of the $\delta^{13}C$ fluxes. We follow with experiments of linear carbon release and three scenarios of carbon uptake during Termination I to investigate the importance of the time scale for the Keeling plot interpretation.

Fast terrestrial carbon release

This would be the scenario closest to the original Keeling plot analysis in terrestrial ecosystem research. There is a source (terrestrial biosphere) which emits CO_2 directly to the atmosphere. In this experiment, the 10 PgC release first increases pCO_2 by more than 4 μatm immediately after the release, and equilibrates to less than 1 μatm higher than initially (Fig. 6a). The $\delta^{13}C$ signal shows a drop by more than 0.3‰ in year one, and a steady state which is nearly similar to the initial situation (Fig. 6a). Near steady state (± 0.1%) in both pCO_2 and $\delta^{13}C$ was reached 376 years after the carbon release.

There are several possibilities to draw a regression function through the Keeling plot (Fig. 6b):

1. A line connecting only the data prior to the start of the carbon release experiment (year 0) and one year later after 10 PgC are released but before any carbon is taken up by the ocean representing the maximum possible slope. Thus, pCO_2 and $\delta^{13}C$ after the release can also be calculated following the mass balance equations of a two reservoir system (Eqs. 3 and 4).

2. A straight line through two points characterising the states prior to the carbon release and after re-equilibration. This would contain the minimum information retrievable in case of low sampling frequency and would be the analog to the theoretical considerations for a three reservoir system.

3. A regression function through the subset of points covering the equilibration process, in which the main dynamics of the carbon release are represented. We here choose all points after the release (year 1) until both pCO_2 and $\delta^{13}C$ were within ±0.1% of their final steady state values.

It is also of interest if and how the amplitude of the carbon release and its isotopic signature influence the Keeling approach. We therefore performed additional simulations (Figs. 6b, d) with smaller amplitude (5 PgC) and different $\delta^{13}C$ signature (−13.5‰, −23.4‰, −33.4‰). These signatures are the result of the variation of the assumed global terrestrial fractionation factor $\varepsilon_{TB}=-17‰$ by ±10‰.

If such an event of terrestrial carbon release is to be detected in ice cores, we have to manipulate our artificial data set to account for both the temporal integral during gas enclosures and the limited sampling frequency. We assumed an average mixing time (running average of 300 years), and a regular sampling frequency of 100 years, typical for Antarctic ice core studies.

A summary of calculated y-axis intercepts is found in Table 2. In the original model output, the regression model 1 (analysis of the carbon flux in the year of the release) can explain the $\delta^{13}C$ signature of terrestrial release very well, independent of amplitude or the $\delta^{13}C$ signature itself. The slight overestimation of the regression model of up to 0.5‰ might be due to numerical limitations. Differences in the y-axis intercept between scenarios with varying amplitude and $\delta^{13}C$ signature of the released carbon are still large in regression model 3 (y_0 from −18.7‰ to −26.0‰), but a simple functional relationship between y-axis intercept y_0 and the $\delta^{13}C_{rel}$ signature of the flux is missing. In model 2 the different $\delta^{13}C$ signatures of the carbon release flux are still distinguishable by small differences in the y-axis intercept (y_0=−7.5‰, −8.4‰, −9.3‰). These

y_0's gained from model 2 are similar to the boundary $\delta^{\Delta A}_{\delta C \to 0}$ introduced in Sect. 4, which is an embedded feature of the system configuration. Interestingly, the y_0 values derived from the BICYCLE simulations are about 1‰ isotopically heavier than in our equilibrium model in Sect. 4. The reason for this is the establishing of vertical gradients in DIC and $\delta^{13}C$ in the ocean due to the ocean carbon pumps (Volk and Hoffert, 1985) leading to an enrichment of $\delta^{13}C$ in the surface water by about 1‰.

If we take the signal broadening through temporal mixing in the firn into account (Fig. 6 bottom), the perturbations in pCO_2 and $\delta^{13}C$ are largely reduced to 34% and 7% of their original amplitudes, respectively, and the duration of the atmospheric pCO_2 rise of one year in the original data is now spread over the time length of the smoothing filter (300 yr). Even for conditions similar to those found at Law Dome where the air is mixed only over a time interval of 20 years, the amplitudes in pCO_2 and $\delta^{13}C$ are reduced to 70% and 47% of their original values, respectively. Y-axis intercepts for the 300 years smoothing filter are reduced significantly for regression models 1 (30% to 57% of y_0 in original data) and 3 (48% to 74% of y_0 in original data).

A further increase of uncertainty arises if we reduce the sampling interval. The effect of a 100 year sampling frequency reduces y-axis intercepts calculated with regression model 1 and 3 further (Table 2). However, the uncertainty introduced by reduced sampling frequency is much smaller than the one based on firn air mixing. Results obtained with regression model 2 (boundary $\delta^{\Delta A}_{\delta C \to 0}$) were not affected by any of the two post simulation procedures.

From these fast carbon release experiments, several conclusions can be drawn:

1. The results of regression model 1 are in line with the mass balance equations of the two reservoir Keeling approach.

2. In all multi-annual experiments the oceanic uptake of carbon will play an important role.

3. Fast terrestrial carbon release events are in their full extent not recordable in the ice core records due to the time integral introduced by the firn enclosure process.

Slow terrestrial carbon exchange

To understand glacial/interglacial dynamics one has to investigate larger varia-
tions in terrestrial carbon storage of several hundreds of PgC, which occurred over
longer time intervals. We have therefore performed additional experiments, one in
which 500 PgC is released by the terrestrial pools, but now with a constant release
rate over a period of 6000 years. In a second set of experiments we mimic in a
simplistic way the carbon uptake of approximately 400 PgC over 6000 yr which might
have occurred during the last glacial/interglacial transition between 18 and 12 kyr BP
as assumed in three different scenarios (TB0, TB1, TB2) in Köhler et al. (2005a).
These scenarios differ in functional dependencies of the terrestrial carbon storage on
CO_2 fertilisation and climate change (TB0: linear rise in terrestrial carbon; TB1: mainly
CO_2 dependent; TB2: mainly climate dependent; Fig. 7).

In both linear experiments (carbon release and TB0) the atmospheric $\delta^{13}C$ record
shows a relaxation behaviour in the first several hundred years after the beginning
and after the end of the carbon release with a gradual change in between (Fig. 8).
Atmospheric pCO_2 is changing rather constantly over time, also with small nonlinear
responses in the first few hundred years at the beginning and at the end of the exper-
iment. These discontinuities are caused by the time-delayed oceanic carbon uptake.
For example, after the end of the experiment ($t=6$ kyr, Fig. 8a) large parts of the re-
leased carbon are taken up by the ocean in the following centuries, similar as in the
fast carbon release experiment shown in Fig. 6. In the more complex scenarios TB1
and TB2 the changes in pCO_2 and $\delta^{13}C$ are largest in the climate dominated sce-
narios TB2 with changing rates of up to 30 μatm in pCO_2 and 0.3‰ in $\delta^{13}C$ in 1000
years. In the Keeling plots the relaxation behaviour at the beginning and the end of
the linear experiments leads to offsets from the well defined linear relationship. A re-
gression over the whole time period leads to a $y_0=-8.6$‰, only 0.2‰ smaller than the
$\delta^{\Delta A}_{\delta C \to 0}$ boundary for this system. The scatter of the data points is larger in TB1 and
TB2 than in the linear experiments, but the regression model through the data is still

very good ($r^2 \geq 94$%) leading to $y_0=-9.1$‰ and -9.0‰, respectively. The slope of the
regression is steeper here, because the fractionation factor of the terrestrial biosphere
ε_{TB} is changing over time. The fraction of terrestrial carbon produced by C_4 photosyn-
thesis is decreasing from ~30% during the LGM to ~20% during preindustrial times
in the scenarios TB1 and TB2 (Köhler and Fischer, 2004). This leads to a terrestrial
fractionation which is more than 1‰ more negative in the preindustrial times than in
the LGM.

The range of the $\delta^{13}C$ values concluded from our simulation results for a slow ter-
restrial carbon release agrees well with the ones proposed by our theoretical three
reservoir approach in Sect. 4 and is very different from the original $\delta^{13}C$ of the car-
bon source. It is especially remarkable that the differences of the y_0's from $\delta^{\Delta A}_{\delta C \to 0}$
are very small. Furthermore, these slow carbon exchange processes are so slow that
the air enclosure procedure with the assumed smoothing filter of 300 years would only
marginally alter the records and would not change the y_0 values. Similarly the restricted
sampling frequency is of no importance here. These two processes will therefore not
be analysed any further in the following, because it is reasonable to assume that their
impact on the observed processes can be neglected.

5.3.2 Marine biosphere

While the marine biosphere is in principle a reservoir separate from DIC in the ocean
and the atmospheric carbon, it is not independent because the marine export produc-
tion establishes vertical gradients in DIC and $\delta^{13}C$ between the surface and the deep
ocean. Accordingly, the following discussion of changes caused by the marine bio-
sphere and other factors represents already a misuse of the Keeling plot approach.
Nevertheless it is instructive to study whether the end member analysis can lead to
meaningful results and is able to distinguish between different processes.

For the marine biota we again first want to explore the range of possible results be-
fore we analyse one scenario which seems to be realistic for the last glacial/interglacial

transition. We therefore concentrate first on a switch from an abiotic ocean without any marine biological productivity and no export production to a biotic ocean in year 0 and vice versa. After these biotic/abiotic experiments, the possible effect of an extended glacial marine productivity due to the iron fertilisation in the Southern Ocean is explored. In the biotic ocean a flux of $10\,\mathrm{PgC\,yr^{-1}}$ of organic carbon is exported at 100 m water depth to the deeper ocean. This organic export production is coupled via the rain ratio to an export of $1\,\mathrm{PgC\,yr^{-1}}$ of inorganic $CaCO_3$.

The abiotic/biotic switch leads to a decrease in atmospheric pCO_2 of about 220 μatm and a rise in atmospheric $\delta^{13}C$ of 1.0‰ (Fig. 9a) and the opposite signals in the biotic/abiotic experiment (not shown). The iron fertilisation experiment decreases glacial pCO_2 by 20 μatm, in parallel with a 0.15‰ rise in $\delta^{13}C$ (Fig. 10a). Here, both atmospheric records are relaxing to their preindustrial values after the onset of iron limitation around 18 kyr BP. The Keeling plot analysis leads to y-axis intercepts of −8.0 to −10.2‰ for the three different regression models in the abiotic/biotic experiment (Fig. 9b). Comparing only the prior/after model for all three experiments (abiotic/biotic, biotic/abiotic, iron fertilisation) (Figs. 9b, 10b) gives nearly identical results (y_0=−8.7±0.1‰). If the time window of analysis is reduced to the first 50 years after the beginning of the reduction in export production in the iron fertilisation experiment a steeper slope in the Keeling plot leads to y_0 of −9.7‰ (Fig. 10b).

The marine export production combines two of the three ocean carbon pumps: the organic or soft-tissue pump and the carbonate pump (Volk and Hoffert, 1985). The third one, the solubility pump, operates by the increased solubility of CO_2 in downwelling cold water. They all introduce vertical gradients in DIC in the water column, the biological pumps additionally build up a gradient in $\delta^{13}C$. DIC is reduced in the surface layers through marine production of both organic material (soft-tissues) and $CaCO_3$ and increased in the abyss through carbon released during remineralisation and dissolution. During photosynthesis $\delta^{13}C$ is depleted by about −20‰, thus leaving carbon enriched in ^{13}C at the surface, while the exported organic matter is depleted. The isotopic fractionation during the production of hard shells slightly enriches ^{13}C in

535

the carbonate ($\varepsilon \in$[0‰,3‰]). The vertical gradient in $\delta^{13}C$ leads to a difference of about 1.0‰ between surface (1.5‰) and abyss (0.5‰) in the biotic ocean, while the $\delta^{13}C$ signal in the abiotic ocean does not change with depth and is around 0.55‰. If we now switch on the marine production in a formerly abiotic ocean we merely introduce these gradients to the system. Surface $\delta^{13}C$ is rising by 1.0‰ and so is the atmospheric $\delta^{13}C$. The signal seen in the atmospheric record is therefore a mixture of the fractionation during gas exchange and an increased carbon flux from the atmosphere to the ocean. In BICYCLE the flux of CO_2 from the surface ocean to the atmosphere has a fractionation factor of $\varepsilon_{O2A} \approx -10.4$‰ and $\varepsilon_{A2O} \approx -2.4$‰ in the opposite direction leading to a net fractionation effect of −8.0‰ (but both depend also on temperature, and ε_{O2A} additionally on DIC, HCO_3^-, and CO_3^{2-}). Similar as in the previous case of a terrestrial carbon release the system contains a boundary in the effective isotopic signature. Each perturbation of the system leads to a derivation from this boundary. The effects of changes in the marine carbon fluxes on atmospheric pCO_2 and $\delta^{13}C$ are not necessary the same as for the terrestrial case. Therefore, the boundary is not identical with $\delta^{\Delta A}_{\delta C \to 0}$, but seems to be very close. From variations of the global export production one can estimate this marine boundary to be around −8.5‰. In year 1, for example, one can understand the signal (y_0=−10.2‰) in the following way: In areas in which marine export production is reducing surface DIC the gross carbon flux from the ocean to the atmosphere is largely reduced. In the most extreme case we would only find a gross carbon flux from the atmosphere to the ocean with the corresponding fractionation factor ε_{A2O}=−2.4‰. This would be the isotopic signature of the process in action and added to the marine boundary it would lead at maximum to a y_0 of −10.9‰. The calculated y_0 is smaller because there is still a small but not negligible gross flux of CO_2 from the ocean to the atmosphere. The signal during the first 50 years of the iron fertilisation experiment (y_0=−9.7‰) can be interpreted similarly. During the latter part of the abiotic/biotic switch experiment and over the equilibration period y_0 is ∼−8.0‰ and thus more positive than the marine boundary. This might be caused by the increased $\delta^{13}C$ of the DIC in the surface waters. After 100 years, pCO_2 has already

536

dropped to 346 μatm, thus nearly 2/3 of the oceanic uptake of carbon happens in this first century. Therefore the carbon fluxes from the atmosphere to the ocean and vice versa are nearly similar thereafter. That means that now the isotopic enriched DIC of the surface waters can enter the atmosphere and is then enriching $\delta^{13}C$ and y_0.

If compared with the terrestrial experiments the results from regression model 3 (prior/after analysis) have y_0's which are only 0.2 to 0.4‰ more negative than $\delta^{\Delta A}_{\delta C \to 0}$. This is very similar to the experiments with slow carbon exchange between the terrestrial biosphere and the atmosphere.

5.3.3 Ocean circulation

Previously Köhler et al. (2005a) assumed a rise in the strength of the North Atlantic Deep Water (NADW) formation from 10 Sv (10^6 m^3 s^{-1}) during the Last Glacial Maximum (LGM) to intermediate levels of 13 Sv in the Bølling/Allerød warm interval and 16 Sv at the beginning of the Holocene. This rise was punctuated by sharp drops in the NADW formation strength and the subsequent ocean circulation fluxes to 0 Sv and 11 Sv during the Heinrich 1 event and the Younger Dryas, respectively. Repeating this temporal sequence of events over a period of approximately 6000 years leads to drops in pCO_2 by 10 μatm during times of reduced ocean circulation accompanied by rises in $\delta^{13}C$ of about 0.05‰. Initial and final values differ by about 15 μatm and −0.05‰ (Fig. 11a).

The prior/after analysis in the Keeling plot leads to a y-axis intercept of −7.8‰, however, the pattern is highly time-dependent and allows a breakdown of the time series into the individual events, which show distinctively different behaviour. These events are marked in Figs. 11a, b (1: decrease in NADW formation during Heinrich 1 event; 2: increase in NADW formation during Bølling/Allerød warm interval; 3: decrease in NADW formation during Younger Dryas; 4: increase in NADW formation towards interglacial levels). The regression analysis over the whole of these four periods, which last between 1200 and 2000 years each, finds y-axis intercepts between −5.3 and −7.2‰.

If shorter time windows after the beginning of these changes in ocean circulation are analysed, much steeper regression functions can be found. For example, the regressions through 50 year time windows at the beginning of interval 2 and 4, which show the steepest slopes in the Keeling plot, lead to y-axis intercepts of −39.1 and −9.5‰, respectively (Fig. 11b).

The complete shut-down of the NADW formation during Heinrich 1 event alters also the nutrient availability for the marine biota. The export of organic matter depends on the availability of macro-nutrients in the surface waters and is prescribed to an upper limit of 10 PgC yr^{-1}. In the time interval between 16.5 and 15 kyr BP marine export falls from 10 PgC yr^{-1} to 8.9−9.3 PgC yr^{-1}. Less export production increases atmospheric pCO_2 and decreases atmospheric $\delta^{13}C$. This implies that the peaks in the atmospheric carbon records were both dampened during interval 1. Accordingly, the y_0 derived from the Keeling plot during this time interval is a mixture of ocean circulation and marine biota.

A second ocean circulation process which changed according to Köhler et al. (2005a) over the time of the last transition was the Southern Ocean vertical mixing rate (Figs. 11c, d). It rose from 9 Sv (glacial) to 29 Sv (preindustrial) and led to a rise in pCO_2 by about 30 μatm and a drop in $\delta^{13}C$ by more than 0.2‰. Here, the Keeling plot interpretation gives us a y-axis intercept of −8.2‰ for the prior/after analysis. The steepest slope during the first 50 years after the start of the change would yield to a y-axis intercept of −11.0‰ (Fig. 11d).

The overturning circulation distributes carbon in the ocean. Its effect on the atmospheric carbon reservoirs, however, is opposite to that of the three ocean carbon pumps. While the pumps introduce vertical gradients in DIC and $\delta^{13}C$ as described in the subsection about the marine biota, the overturning circulation is reducing these vertical gradients again through the ventilation of the deep ocean which brings water rich in DIC and depleted in ^{13}C back to the surface. A weakening of the ventilation reduces these upwelling processes and leads to lower pCO_2 and higher $\delta^{13}C$ values as seen in the experiments.

The y_0-values derived from the four intervals for changing NADW formation differ. Between interval 3 and 4 in which opposing changes in ocean circulation occur, the differences in the y_0-values are small. These different circulation patterns can be seen in the Keeling plot in the dynamics of the first years of the intervals: In intervals 1 and 3, in which the strength of the NADW formation is reduced, the analysis of a time window at the beginning of the interval leads to less negative y_0 than over the whole period, while the opposite is the case in the intervals 2 and 4 with a resumption of the NADW formation. These temporal changes over the course of each interval are caused by the equilibration of the model to a new steady state. In interval 1, the shutdown of the NADW and the subsequent fluxes lead first to an enrichment of DIC and of ^{13}C in the North Atlantic surface waters and thus to higher atmospheric δ^{13}C. Later-on, this is over-compensated by decreasing DIC and δ^{13}C in the equatorial surface of the Atlantic Ocean. However, the dynamics during a complete shutdown of the NADW formation might be unrealistic because in the current model configuration the tropical Atlantic surface and intermediate ocean boxes would exchange water with each other but not with any other water masses (Fig. 4). This artefact is also responsible for the dynamics during the first years of interval 2, but is not affecting the latter intervals.

Compared to the terrestrial carbon release we can say that a change in ocean circulation is assigned to a y_0 slightly more positive than the terrestrial boundary $\delta^{\Delta A}_{\delta C \to 0}$ (+0.2 to +1.2‰). The dynamics during the first years of a abrupt rise/decrease in the strength of the overturning circulation lead to larger offsets (fall/rise) from the terrestrial boundary.

5.3.4 Gas exchange/sea ice

A change in sea ice cover leads to changes in the gas exchange rates with opposing effects for the northern and the southern high latitudes. As the preindustrial North Atlantic Ocean is a sink for CO_2 a reduced gas-exchange due to higher sea ice cover leads to rising atmospheric pCO$_2$, while the same happening in the Southern Ocean being a source for CO_2 leads to a drop in pCO$_2$. Again, we first explore the maximum

amplitudes possible by covering either the whole North Atlantic Ocean or Southern Ocean surface boxes with sea ice, reducing the gas exchange rates in these areas to zero (Fig. 12 top) before we investigate a data-based scenario for Termination I in which sea ice was approximately doubled during glacial times (Fig. 12 bottom).

In the extreme scenarios sea ice cover is relaxed instantaneously from a full coverage of the surface ocean boxes to preindustrial areal distribution in year 0. The experiment in the North Atlantic yields a drop in pCO$_2$ by 35 μatm, a drop in δ^{13}C by 0.04‰, and a y-axis intercept (prior/after analysis) in the Keeling plot analysis of −6.1‰. A similar experiment in the Southern Ocean increases pCO$_2$ by about 15 μatm, δ^{13}C drops by 1.0‰ leading to a prior/after y-axis intercept of −23.8‰.

In the data based scenario across Termination I the annual averaged sea ice area during LGM is approximately doubled (Crosta et al., 1998a,b; Sarnthein et al., 2003; Gersonde et al., 2005) and its evolution is coupled to sea surface temperature changes. pCO$_2$ fluctuates by about 10 μatm and δ^{13}C by 0.15‰ (Fig. 12c). Due to the different responses in the North and in the South the data plotted as Keeling plot zig-zag quite a lot. Prior/after analysis finds an y-axis intercept of −0.7‰. The regression over the whole period finds $y_0 = -3.8$‰ ($r^2 = 38\%$). The data based contribution from the North ($y_0 = -4.8$‰) and the South ($y_0 = -77.2$‰) have very different y-axis intercepts (Fig. 12d).

The very negative y_0 caused by changes in sea ice coverage in the Southern Ocean needs further clarification. The changes in sea ice coverage cause variations in the gas exchange rates. In the scenario across Termination I, the global exchange flux rises from 52 PgC yr^{-1} during the LGM to 58 PgC yr^{-1} at $t = 10$ kyr BP in the scenario, which considers only changes in sea ice in the Southern Ocean. The pCO$_2$ of the atmosphere and the Southern Ocean surface box are very close to each other at the beginning of the experiment (270 and 266 μatm, respectively). Therefore, an increase in gas exchange rate in the Southern Ocean is only marginally increasing atmospheric pCO$_2$ (<1 μatm). However, the stronger gas exchange leads to a significant decrease in atmospheric δ^{13}C by 0.08‰. A y_0 of −77.2‰ is consistent in our modelling envi-

ronment, but dependent strongly on the model architecture. In general, the effects of sea ice coverage on carbon cycle dynamics have been found to vary between different models (Archer et al., 2003). This example shows, that the Keeling plot is difficult to interpret for experiments without significant net carbon uptake or release of the atmo-
5   sphere, which lead nevertheless to changes in atmospheric δ^{13}C. The slope of the regression function might in the most extreme case of a constant pCO$_2$ rise to infinity. Besides gas exchange a second example for this situation is a change from C3 grasses to C4 grasses in the terrestrial biosphere.

The difference of these results from $\delta^{\Delta A}_{\delta C \rightarrow 0}$ gives us a comparison with the terrestrial
10   release scenario. The contribution from changing gas exchange in the Arctic carries a y_0 several ‰ heavier than $\delta^{\Delta A}_{\delta C \rightarrow 0}$, while fast changes in the gas exchange in the South lead to lighter y_0.

5.3.5   Sea level and ocean temperature

Changes in sea level and ocean temperature over the last glacial/interglacial transition
15   are documented rather well in the paleo climate archives. We therefore describe in the following only those changes which we propose over Termination I, but do not analyse the maximum range possible by these two processes.

Sea level

20
Sea level rose from 20 kyr BP to 10 kyr BP by about 85 m (Fairbanks, 1990). This leads in our model to a drop in pCO$_2$ by about 13 μatm and nearly no change in the δ^{13}C. The y-axis intercept in a Keeling plot with prior/after analysis or regression over whole time period is −6.4‰ (Fig. 13 top).
25   The rising sea level leads to a dilution of the concentration of all species in the ocean and a decrease in salinity by about 2.3%. The ocean can then store more carbon. Again, in the comparison with the terrestrial case this sea level rise is a process with a

typical δ^{13}C signature that is about +2‰ more positive than $\delta^{\Delta A}_{\delta C \rightarrow 0}$.

Ocean temperature

5   The rise of the ocean temperature by 3 to 5 K during the simulated 10 kyr (20 to 10 kyr BP) leads to a rise in pCO$_2$ of 32 μatm, and a rise in δ^{13}C of 0.4‰, the latter leading the first by about 1000 years (Fig. 13 bottom). The Keeling plot analysis gives us y_0's of −3.5 and −3.6‰ for the regression over the whole period and the prior/after analysis, respectively.
10   Due to the temperature dependent solubility of CO$_2$ warm water stores less carbon than cold water. A rise in ocean temperature therefore weakens the solubility pump and leads to an out-gassing of CO$_2$. The rise in δ^{13}C is mainly caused by the temperature-dependent isotopic fractionation during gas exchange between the surface ocean and the atmosphere. The temperature effect has a δ^{13}C signature which is about +5‰
15   heavier than the $\delta^{\Delta A}_{\delta C \rightarrow 0}$ obtained in the terrestrial release case.

5.3.6   Combined scenarios and CaCO$_3$ chemistry

The previous study (Köhler et al., 2005a) finds that combined scenarios are able to re-construct the observed dynamics in atmospheric pCO$_2$ and δ^{13}C during Termination I (Fig. 15). They combine the processes investigated above (terrestrial carbon storage,
20   marine biology, ocean circulation, temperature, sea level, sea ice) together with the consideration of CaCO$_3$ fluxes between sediment and ocean.

The influence of the fluxes of CaCO$_3$ cannot be analysed separately as CaCO$_3$ fluxes between deep ocean and sediment are generated by the model as response to changes in the deep ocean CO$_3^{2-}$ concentration. CaCO$_3$ chemistry is acting as an
25   amplifier of the results of all other processes with respect to the changes in pCO$_2$. However, we can estimate their impact by subtracting the results of a simulation which includes all processes apart from sediment/ocean fluxes from the results of a scenario

including all processes. Over the course of Termination I the sedimentation of $CaCO_3$ is higher than its dissolution, leading to a loss of DIC ($\sim$1000 PgC) and twice as much alkalinity. These changes lower the pH of the ocean, which shifts the distribution of the three different species of DIC (CO_2, HCO_3^-, CO_3^{2-}) in the carbonate system towards CO_2, and leads to its out-gassing and a rise in atmospheric pCO_2 of approximately 35 μatm (Fig. 14a). This loss of carbon is accompanied by a depletion of the mean oceanic $\delta^{13}C$ by about 0.1‰, because the $CaCO_3$, which is lost to the sediments bears a $\delta^{13}C$ signal of about 3‰. Atmospheric $\delta^{13}C$ is therefore falling by approximately the same amount. If the $\delta^{13}C$ record is corrected for this effect of sedimentation, it rises by about 0.2‰ (Fig. 14). This residual rise is caused by the fractionation factor of the CO_2 flux from the ocean to atmosphere, which depends on DIC itself and the pH dependent dissociation of DIC into the different species (Ridgwell, 2001). The Keeling plot analysis of these changes (Fig. 14b) leads to y_0 of −5.8‰ and −5.2‰ for both the prior/after analysis and the regression model of the original and the corrected data, respectively.

Termination I was subdivided into four intervals based on different changing rates in the CO_2 record (Monnin et al., 2001). Depending on the realisation of the variation of the terrestrial carbon storage over time, three different scenarios are discussed (A-TB0, A-TB1, A-TB2; Fig. 7). In the Keeling plot of these combined results the only well distinct feature found in all three scenarios is the sharp drop in $\delta^{13}C$ in parallel with rising pCO_2 which occurs during interval I, 18–16.5 kyr BP (Fig. 15b). In the Taylor Dome data set this is also the only event in which the signal-to-noise-ratio is high enough to allow a distinct identification. Changes in interval II (16.5–15 kyr BP) and III (15–13 kyr BP) occur during rather small or no variations in pCO_2 leading to features which are rather indistinguishable in the light of their uncertainties in the data sets. The scenario A-TB2 shows a variability in $\delta^{13}C$ which is closest to that of the Taylor Dome record, while pCO_2 is best reconstructed in the A-TB0 simulation.

In the following we have a closer look on the Keeling plots of these three combined scenarios and especially on the results of A-TB2 (Figs. 15b, 16). Regression functions

are applied to seven time windows in scenario A-TB2 (Table 4, Fig. 16b):

1. The main dynamics of a reduced marine export production due to iron limitation falls in time window 1 (20.0–17.1 kyr BP). In the combined scenario y_0 is −7.3‰ while the decrease in export production as single process would lead to y_0=−8.6‰ with at maximum −9.7‰ during the first years of the reduced export production.

2. The increase in Southern Ocean vertical mixing is mainly happening in window 2 (17.0–16.9 kyr BP) leading to y_0=−10.0‰ in A-TB2, but to −8.2‰ as single process.

3. There is no specific process in operation in window 3 (16.8–16.6 kyr BP) which has a y_0 of −5.2‰.

4. In window 4 (16.5–14.9 kyr BP) covering the Heinrich 1 event the NADW formation is shut-off. Additionally, the marine export production is reduced by $\sim$10% due to macro-nutrient limitation.

5. NADW formation is resuming to intermediate strength in time window 5 covering the beginning of the Bølling-Allerød warm interval in-between Heinrich 1 and the Younger Dryas (14.8–14.3 kyr BP). From a comparison of the three scenarios (Fig. 15b) we further know that the changing carbon storage in the terrestrial biosphere is additionally affecting the time windows 4 and 6, and that it is mainly responsible for the dynamics in time window 5. In the scenarios A-TB0 and A-TB1 the time windows 4 and 5 are not distinguishable.

6. In the Younger Dryas (window 6, 14.2–11.8 kyr BP) the NADW formation is partly reduced.

7. No clear regression (r^2=6%) is found for window 7 (11.7–10.0 kyr BP), in which the carbon cycle is organised to a new interglacial equilibrium.

A-TB2 leads to y-axis intercepts of −11.4‰, −13.3‰, and −13.0‰ in the windows 4, 5, and 6 respectively. For comparison, the single process analysis has found $y_0 = -5.3$‰ to −7.2‰ for changes in NADW formation between 16.5 and 11.8 kyr BP, but much higher negative values (−39.2‰) in certain times. The rise in the terrestrial carbon storage has $y_0 = -8.6$ to −9.1‰.

This analysis above shows that it seems possible to identify single processes in the Keeling plot of our artificial time series, if they dominate the atmospheric carbon records for a certain time. However, due to the variety of the processes the y-axis intercept which we identify in the combined scenarios is in no case near or close to the expected y_0 values we concluded from our single process analysis.

6 Discussion and conclusions

In this study we analysed processes which alter the atmospheric content of carbon dioxide and δ^{13}C of CO_2 using artificial time series produced with a global carbon cycle box model. Although there is evidence that the scenarios investigated here are plausible and they can explain the observations during the last glacial/interglacial transition, alternatives can not be ruled out due to data uncertainties and model simplicity. Nevertheless, for the investigation of these artificial time series and their potential to be interpreted using the Keeling plot approach, the absolute validity of these scenarios is not important. By using a simple carbon cycle model we benefit from the fact that individual processes acting on the carbon cycle can be switched on and off and their hypothetical impacts can be analysed individually.

All processes have been analysed with respect to their impact to the Keeling plot analysis. A summary is found in Table 3. The effective isotopic signature $\delta^{\Delta A}$ of terrestrial carbon uptake or release modifying the global carbon cycle can be understood based on theoretical considerations of a three reservoir system which also includes oceanic carbon uptake. These considerations can be understood as the paleo extension of the Keeling plot approach. The effective isotopic signature converts to a

boundary $\delta^{\Delta A}_{\delta C \to 0}$ of −8.4‰ for terrestrial carbon fluxes approaching zero. The $\delta^{\Delta A}_{\delta C \to 0}$ obtained from theory is comparable to the y-axis intercept y_0 in a classical Keeling plot. We identified y-axis intercepts of different processes and compared it with the theoretical well understood value of the terrestrial carbon release. The y_0's of the prior/after analysis of our single process analysis vary between −0.7 and −8.6‰. Some processes are compounds of subprocesses which have distinctively different y_0 values (e.g. sea ice cover in different hemispheres, y_0 (north)=−4.8‰; y_0 (south)=−77.2‰), in others the prior/after analysis leads to very different results if a specific narrow time window is observed (e.g. terrestrial carbon storage, NADW formation). Furthermore, the terrestrial carbon storage very likely changed in a non-linear way during the last glacial/interglacial transition and not in a linear way as assumed in scenario TB0 (Fig. 7). This is also supported by a simulation studies using a dynamical global simulation model (Köhler et al., 2005b). High frequency changes on a centennial to millennial time scale are very likely smoothed out in the ice core records due to the average mixing time of the air of several centuries and the limited sampling frequency. The single process analysis of the states prior and after the experiments leads to y_0 different than the boundary caused by terrestrial processes. They vary from $\delta^{\Delta A}_{\delta C \to 0}$ by a small decline (−0.2‰) to a large increase (+7.7‰). Processes in which the biology is involved (marine and terrestrial) have identical y_0's (small decline in comparison to $\delta^{\Delta A}_{\delta C \to 0}$) and are therefore indistinguishable. In all other cases y_0 is more positive than $\delta^{\Delta A}_{\delta C \to 0}$.

The Taylor Dome record of atmospheric δ^{13}C shows dynamics, in which a Keeling plot analysis leads to y_0 values around −9.5‰ (Smith et al., 1999; Fischer et al., 2003). This holds, however only for the Holocene and the climatically relatively stable LGM, while during the transition no clear end member could be recognised so far. Unpublished measurements (Eyer, 2004) performed at the EPICA Dome C ice core show evidence for millennial scale variability with fast and large changes in δ^{13}C (more than 0.5‰ in a century). We believe from our analysis that the processes responsible for

these variations can not be identified based on a Keeling plot analysis. However, our study gives us some indications which processes could contribute to fast changes and thus might be responsible for very negative y-axis intercepts in a Keeling plot analysis. From what we have learned from our model of the global carbon cycle fast changes in terrestrial carbon storage, variations in ocean circulation strength (NADW formation) and sea ice coverage in the Southern Ocean are the only processes which can contribute significantly to these δ^{13}C excursions. However, the signal of fast terrestrial carbon release is smoothed by air mixing processes in the firn. In the EPICA Dome C ice core with its small accumulation rate and large mixing time terrestrial processes might therefore not be responsible for these negative δ^{13}C signals.

In the light of these conclusions we have to acknowledge that especially the modelling response to Southern Ocean sea ice extent is highly model dependent. Large variability in pCO$_2$ and δ^{13}C occur especially when the surface ocean box is nearly fully covered with sea ice and thus reducing gas exchange dramatically (Köhler and Fischer, 2006). Thus, our model architecture with a Southern Ocean box ranging from 40°S to the Antarctic continent is probably too simplistic to cover the complete picture of observed dynamics. Other model intercomparisions have already pointed out these model-dependent behaviour (Archer et al., 2003).

From the understanding which emerges here, it seems unlikely, that the interpretation of δ^{13}C measured during glacial/interglacial transitions can be enhanced very much with the Keeling plot approach. The identification of a single process which might be responsible for the observed fluctuations in atmospheric CO$_2$ and δ^{13}C can not be based on a Keeling plot analysis. Most processes acted simultaneously on the global carbon cycle during the transition and the uncertainties in data retrieval, y-axis intercept, and δ^{13}C are too large to come to a sound and unequivocal process identification.

547

References

Archer, D. E., Martin, P. A., Milovich, J., Brovkin, V., Plattner, G.-K., and Ashendel, C.: Model sensitivity in the effect of Antarctic sea ice and stratification on atmospheric pCO$_2$, Paleoceanography, 18, 1012, doi:10.1029/2002PA000760, 2003. 541, 547

Blasing, T. J., Broniak, C., and Marland, G.: Estimates of monthly carbon dioxide emissions and associated δ^{13}C values from fossil-fuel consumption in the U.S.A, in: Trends: A Compendium of Data on Global Change, Carbon Dioxide Information Analysis Center, Oak Ridge National Laboratory, U.S. Department of Energy,, Oak Ridge, Tenn., USA, 2004. 520, 526

Bowling, D. R., Tans, P. P., and Monson, R. K.: Partitioning net ecosystem carbon exchange with isotopic fluxes of CO$_2$, Global Change Biology, 7, 127–145, 2001. 517

Brook, E. J., Harder, S., Serveringhaus, J., Steig, E. J., and Sucher, C. M.: On the origin and timing of rapid changes in atmospheric methane during the last glacial period, Global Biogeochem. Cycles, 14, 559–572, 2000. 558

Crosta, X., Pichon, J.-J., and Burckle, L. H.: Application of modern analog technique to marine Antarctic diatoms: Reconstruction of maximum sea-ice extent at the Last Glacial Maximum, Paleoceanography, 13, 284–297, 1998a. 540

Crosta, X., Pichon, J.-J., and Burckle, L. H.: Reappraisal of Antarctic seasonal sea-ice extent at the Last Glacial Maximum, Geophys. Res. Lett., 14, 2703–2706, 1998b. 540

Dansgaard, W., Clausen, H. B., Gundestrup, N., Hammer, C. U., Johnsen, S. F., Kristinsdottir, P. M., and Reeh, N.: A new Greenland deep ice core, Science, 218, 1273–1277, 1982. 529

Emanuel, W. R., Killough, G. G., Post, W. M., and Shugart, H. H.: Modeling terrestrial ecosystems in the global carbon cycle with shifts in carbon storage capacity by land-use change, Ecology, 65, 970–983, 1984. 525

Etheridge, D. M., Steele, L. P., Langenfelds, R. L., Francey, R. J., Barnola, J.-M., and Morgan, V. I.: Natural and anthropogenic changes in atmospheric CO$_2$ over the last 1000 years from air in Antarctic ice and firn, J. Geophys. Res., D101, 4115–4128, 1996. 528

Eyer, M.: Highly resolved δ^{13}C measurements on CO$_2$ in air from Antarctic ice cores, Ph.D. thesis, University of Bern, Bern, Switzerland, 2004. 518, 528, 546

Eyer, M., Leuenberger, M., Nyfeler, P., and Stocker, T.: Comparison of two δ^{13}CO$_2$ records

548

measured on air from the EPICA Dome C and Kohnen Station ice cores, Geophys. Res. Abstr., 6, 01 990, 2004. 528

Fairbanks, R. G.: The age and origin of the Younger Dryas climate event in Greenland ice cores, Paleoceanography, 5, 937–948, 1990. 541

Fischer, H., Wahlen, M., and Smith, J.: Reconstruction of glacial/interglacial changes in the global carbon cycle from CO_2 and $\delta^{13}CO_2$ in Antarctic ice cores, Memoirs of the National Institute for Polar Research, Special Issue, 57, 121–138, 2003. 516, 518, 519, 520, 522, 546

Flanagan, L. B. and Ehleringer, J. R.: Ecosystem-atmosphere CO_2 exchange: interpretating signals of change using stable isotope ratios, Trends in Ecology and Evolution, 13, 10–14, 1998. 517

Francey, R. J., Allison, C. E., Etheridge, D. M., Trudinger, C. M., Enting, I. G., Leuenberger, M., Langenfelds, R. L., Michel, E., and Steele, L. P.: A 1000-year high precision record of $\delta^{13}C$ in atmospheric CO_2, Tellus, 51B, 170–193, 1999. 518, 558

Friedli, H., Lötscher, H., Oeschger, H., Siegenthaler, U., and Stauffer, B.: Ice core record of the $^{13}C/^{12}C$ ratio of atmospheric CO_2 in the past two centuries, Nature, 324, 237–238, 1986. 517

Gersonde, R., Crosta, X., Abelmann, A., and Armand, L.: Sea-surface temperature and sea ice distribution of the Southern Ocean at the EPILOG Last Glacial Maximum – a circum-Antarctic view based on siliceous microfossil records, Quat. Sci. Rev., 24, 869–896, 2005. 540

Hemming, D., Yakir, D., Ambus, P., Aurela, M., Besson, C., Black, K., Buchmann, N., Burlett, R., Cescatti, A., Clement, R., Gross, P., Granier, A., Grünwald, T., Havrankova, K., Janous, D., Janssens, I. A., Knohl, A., Köstner, B., Kowalski, A., Laurila, T., Mata, C., Marcolla, B., Matteucci, G., Moncrieff, J., Moors, E. J., Osborne, B., Pereira, J. S., Pihlatie, M., Pilegaard, K., Ponti, F., Rosova, U., Rossi, F., Scartazza, A., and Vesala, T.: Pan-European $\delta^{13}C$ values of air and organic matter from forest ecosystems, Global Change Biology, 11, 1065–1093, doi:10.1111/j.1365–2486.2005.00 971.x, 2005. 518

Houghton, R. A.: Revised estimates of the annual net flux of carbon to the atmosphere from changes in land use and land management 1850–2000, Tellus, 55B, 378–390, 2003. 519, 559

Johnsen, S. J., Clausen, H. B., Dansgaard, W., Fuhrer, K., Gundestrup, N., Hammer, C. U., Iversen, P., Jouzel, J., Stauffer, B., and Steffensen, J. P.: Irregular glacial interstadials

549

recorded in a new Greenland ice core, Nature, 359, 311–313, 1992. 529

Keeling, C. D.: The concentration and isotopic abundance of carbon dioxide in rural areas, Geochim. Cosmochim. Acta, 13, 322–334, 1958. 516, 517

Keeling, C. D.: The concentration and isotopic abundance of carbon dioxide in rural and marine air, Geochim. Cosmochim. Acta, 24, 277–298, 1961. 516, 517

Keeling, C. D. and Whorf, T. P.: Atmospheric CO_2 records from sites in the SIO air sampling network, in Trends: A Compendium of Data on Global Change, Carbon Dioxide Information Analysis Center, Oak Ridge National Laboratory, U.S. Department of Energy, Oak Ridge, Tenn., USA, 2005. 518, 558

Keeling, C. D., Bollenbacher, A. F., and Whorf, T. P.: Monthly atmospheric $^{13}C/^{12}C$ isotopic ratios for 10 SIO stations, in: Trends: A Compendium of Data on Global Change, Carbon Dioxide Information Analysis Center, Oak Ridge National Laboratory, U.S. Department of Energy, Oak Ridge, Tenn., USA, 2005. 518, 527, 558

Köhler, P. and Fischer, H.: Simulating changes in the terrestrial biosphere during the last glacial/interglacial transition, Global and Planetary Change, 43, 33–55, doi:10.1016/j.gloplacha.2004.02.005, 2004. 525, 534

Köhler, P. and Fischer, H.: Proposing a mechanistic understanding of changes in atmospheric CO_2 during the last 740 000 years, Clim. Past Discuss., 2, 1–42, 2006. 525, 547

Köhler, P., Fischer, H., Munhoven, G., and Zeebe, R. E.: Quantitative interpretation of atmospheric carbon records over the last glacial termination, Global Biogeochem. Cycles, 19, GB4020, doi:10.1029/2004GB002345, 2005a. 524, 525, 529, 533, 537, 538, 542, 564, 567, 568, 569, 570

Köhler, P., Joos, F., Gerber, S., and Knutti, R.: Simulated changes in vegetation distribution, land carbon storage, and atmospheric CO_2 in response to a collapse of the North Atlantic thermohaline circulation, Climate Dynamics, 25, 689–708, doi:10.1007/s00 382–005–0058–8, 2005b. 530, 546

Landais, A., Barnola, J. M., Masson-Delmotte, V., Jouzel, J., Chappellaz, J., Caillon, N., Huber, C., Leuenberger, M., and Johnsen, S. J.: A continuous record of temperature evolution over a sequence of Dansgaard-Oeschger events during Marine Isotope Stage 4 (76 to 62 kyr BP), Geophys. Res. Lett., 31, L22 211, doi:10.1029/2004GL021193, 2004. 530

Lang, C., Leuenberger, M., Schwander, J., and Johnsen, S.: 16°C rapid temperature variation in central Greenland 70,000 years ago, Science, 286, 934–937, 1999. 529

Levin, I., Ciais, P., Langenfelds, R., Schmidt, M., Ramonet, M., Sidorov, K., Tchebakova, N.,

550

Gloor, M., Heimann, M., Schulze, E.-D., Vygodskaya, N. N., Shibistova, O., and Lloyd, J.: Three years of trace gas observations over the EuroSiberian domain derived from aircraft sampling – a concerted action, Tellus, 54B, 696–712, 2002. 517, 519

Marland, G., Boden, T., and Andres, R. J.: Global, Regional, and National CO_2 Emissions, in Trends: A Compendium of Data on Global Change, Carbon Dioxide Information Analysis Center, Oak Ridge National Laboratory, U.S. Department of Energy, Oak Ridge, Tenn., USA, 2005. 519, 559

Meese, D. A., Gow, A., Alley, R., Zielinski, G., Grootes, P., Ram, M., Taylor, K., Mayewski, P., and Bolzan, J.: The Greenland Ice Sheet Project 2 depth-age scale: Methods and results, J. Geophys. Res., 102, 26 411–26 423, 1997. 572

Monnin, E., Indermühle, A., Dällenbach, A., Flückiger, J., Stauffer, B., Stocker, T. F., Raynaud, D., and Barnola, J.-M.: Atmospheric CO_2 concentrations over the last glacial termination, Science, 291, 112–114, 2001. 528, 543, 572

Mook, W. G.: ^{13}C in atmospheric CO_2, Netherlands J. Sea Res., 20, 211–223, 1986. 516

Munhoven, G.: Modelling glacial-interglacial atmospheric CO_2 variations: the role of continental weathering, Ph.D. thesis, Université de Liège, Liège, Belgium, 1997. 525

Pataki, D. E., Ehleringer, J. R., Flanagan, L. B., Yakir, D., Bowling, D. R., Still, C. J., Buchmann, N., Kaplan, J. O., and Berry, J. A.: The application and interpretation of Keeling plots in terrestrial carbon cycle research, Global Biogeochem. Cycles, 17, 1022, doi:10.1029/2001GB001850, 2003. 516, 517, 518

Petit, J. R., Jouzel, J., Raynaud, D., Barkov, N. I., Barnola, J.-M., Basile, I., Bender, M., Chappellaz, J., Davis, M., Delaygue, G., Delmotte, M., Kotlyakov, V. M., Legrand, M., Lipenkov, V. Y., Lorius, C., Pépin, L., Ritz, C., Saltzman, E., and Stievenard, M.: Climate and atmospheric history of the past 420,000 years from the Vostok ice core, Antarctica, Nature, 399, 429–436, 1999. 527

Plattner, G.-K., Joos, F., and Stocker, T. F.: Revision of the global carbon budget due to changing air-sea oxygen fluxes, Global Biogeochem. Cycles, 16, 1096, doi:10.1029/2001GB001746, 2002. 519

Ridgwell, A. J.: Glacial-interglacial perturbations in the global carbon cycle, Ph.D. thesis, University of East Anglia, Norwich, UK, 2001. 543

Sabine, C. L., Feely, R. A., Gruber, N., Key, R. M., Lee, K., Bullister, J. L., Wanninkhof, R., Wong, C. S., Wallace, D. W. R., Tilbrook, B., Millero, F. J., Peng, T.-H., Kozyr, A., Ono, T., and Rios, A. F.: The oceanic sink for anthropogenic CO_2, Science, 305, 367–371, 2004. 522

551

Sarnthein, M., Pflaumann, U., and Weinelt, M.: Past extent of sea ice in the northern North Atlantic inferred from foraminiferal paleotemperature estimates, Paleoceanography, 18, 1047, doi:10.1029/2002PA000771, 2003. 540

Scholze, M., Kaplan, J. O., Knorr, W., and Heimann, M.: Climate and interannual variability of the atmosphere-biosphere $^{13}CO_2$ flux, Geophys. Res. Lett., 30, 1097, doi:10.1029/2002GL015631, 2003. 519, 526

Schwander, J. and Stauffer, B.: Age difference between polar ice and the air trapped in its bubbles, Nature, 311, 45–47, 1984. 528

Schwander, J., Jouzel, J., Hammer, C. U., Petit, J.-R., Udisti, R., and Wolff, E.: A tentative chronology for the EPICA Dome Concordia ice core, Geophys. Res. Lett., 28, 4243–4246, 2001. 528

Siegenthaler, U., Stocker, T. F., Monnin, E., Lüthi, D., Schwander, J., Stauffer, B., Raynaud, D., Barnola, J.-M., Fischer, H., Masson-Delmotte, V., and Jouzel, J.: Stable carbon cycle-climate relationship during the late Pleistocene, Science, 310, 1313–1317, doi:10.1126/science.1120130, 2005. 527, 528

Smith, H. J., Fischer, H., Wahlen, M., Mastroianni, D., and Deck, B.: Dual modes of the carbon cycle since the Last Glacial Maximum, Nature, 400, 248–250, 1999. 516, 518, 520, 522, 546, 558, 572

Steig, E. J., Brook, E. J., White, J. W. C., Sucher, C. M., Bender, M. L., Lehman, S. J., Morse, D. L., Waddington, E. D., and Clow, G. D.: Synchronous climate change in Antarctica and North Atlantic, Science, 282, 92–95, 1998a. 528

Steig, E. J., Morse, D. L., Waddington, E. D., and Polissar, P. J.: Using the sunspot cycle to date ice cores, Geophys. Res. Lett., 25, 163–166, 1998b. 528

Sturm, P., Leuenberger, M., and Schmidt, M.: Atmospheric O_2, CO_2 and δ^{13}C observations from the remote sites Jungfraujoch, Switzerland, and Puy de Dôme, France, Geophys. Res. Lett., 32, L17 811, doi:10.1029/2005GL023304, 2005. 517

Trudinger, C. M., Enting, I. G., Francey, R. J., Etheridge, D. M., and Rayner, P. J.: Long-term variability in the global carbon cycle inferred from a high-precision CO_2 and δ^{13}C ice-core record, Tellus, 51B, 233–248, 1999. 518, 558

Volk, T. and Hoffert, M. I.: Ocean carbon pumps: analysis of relative strengths and efficiencies in ocean-driven atmospheric CO_2 changes, in: The carbon cycle and atmospheric CO_2: Natural variations archean and present, edited by: Sundquist, E. T. and Broecker, W. S., Geophys. Monograph, 32, 99–110, American Geophysical Union, Washington, D.C., USA,

552

1985. 532, 535

Wolff, E. W., Kull, C., Chappellaz, J., Fischer, H., Miller, H., Stocker, T. F., Watson, A. J., Flower, B., Joos, F., Köhler, P., Matsumoto, K., Monnin, E., Mudelsee, M., Paillard, D., and Shackleton, N.: Modeling past atmospheric CO_2: results of a challenge, EOS, 86(38), 341, 345, 2005. 525

Yakir, D. and Sternberg, L. D. S. L.: The use of stable isotopes to study ecosystem gas exchange, Oecologia, 123, 297–311, 2000. 517

Zeebe, R. E. and Wolf-Gladrow, D. A.: CO_2 in Seawater: Equilibrium, Kinetics, Isotopes, Elsevier Oceanography Book Series, vol. 65, Elsevier Science Publishing, Amsterdam, The Netherlands, 2001. 515, 521, 525

Table 1. Analysis of ground truth of the Paleo-Keeling approach: simulating the anthropogenic rise in $p\text{CO}_2$. Experiments with different $\delta^{13}C_{ant}$ signatures of the anthropogenic carbon flux and for two different systems including an active and a passive terrestrial biosphere are analysed. Displayed are the y-axis intercepts y_0 of the Keeling plots and the ratio which is explained by this approach ($y_0/\delta^{13}C_{ant}$).

Mode of the terrestrial bioshere	$\delta^{13}C_{ant}$ (‰)		
	−20	−25	−30
	y_0 (‰)		
passive	−11.8	−13.7	−15.7
active	−9.2	−11.3	−13.5
	$y_0 / \delta^{13}C_{ant}(-)$		
passive	0.59	0.55	0.52
active	0.46	0.45	0.45

Table 2. Terrestrial carbon release of different amplitude and isotopic signature and calculated y-axis intercept based on the original model output, after low-pass filtering of the data with a 300 year running mean, and after data filtering and reducing the data sets to samples every 100 years.

Scenario		y-axis intercept of different regression models (‰) (r^2 in brackets)			
Amplitude of the release (PgC)	isotopic signature $\delta^{13}C_{rel}$ of release (‰)	model 1 rising[a]	model 2 prior – after[b]	model 3 equilibration[c]	equilibration time (yr) for model 3
original model output					
10	−23.4	−23.8 (100)	−8.4 (100)	−18.7 (68)	375
5	−23.4	−23.6 (100)	−8.4 (100)	−22.3 (75)	189
10	−33.4	−33.9 (100)	−9.3 (100)	−26.0 (68)	375
10	−13.5	−13.6 (100)	−7.5 (100)	−11.4 (70)	375
300 yr running mean					
10	−23.4	−8.9 (93)	−8.4 (100)	−10.4 (85)	241
5	−23.4	−8.9 (93)	−8.4 (100)	−13.8 (89)	71
10	−33.4	−10.2 (92)	−9.3 (100)	−12.6 (84)	241
10	−13.5	−7.7 (95)	−7.5 (100)	−8.4 (86)	241
300 yr running mean + data selection every 100 yr					
10	−23.4	−8.6 (100)	−8.4 (100)	−9.1 (100)	150
5	−23.4	−8.6 (100)	−8.4 (100)	not detectable[d]	50
10	−33.4	−9.6 (100)	−9.3 (100)	−10.5 (100)	150
10	−13.5	−7.5 (97)	−7.5 (100)	−7.7 (100)	150

[a] This covers data during rise of atmospheric pCO_2, which are only two points in the original data set, but longer series in smoothed records.
[b] Comparing steady state before with new steady state after carbon release.
[c] Regression during declining pCO_2 in equilibration time.
[d] There is only one data point in the time window spanned by the equilibration process, from which no regression analysis can be performed.

555

Table 3. Summary of y-axis intercept y_0 and its difference from the terrestrial boundary $\delta_{\delta C \to 0}^{\Delta A} = -8.4‰$ of the prior/after Keeling plot analysis for processes changing over Termination I.

Process	y_0 (‰)	$y_0 - \delta_{\delta C \to 0}^{\Delta A}$ (‰)	Comment
Linear rise in terrestrial carbon storage	−8.6	−0.2	increase was probably non-linear, steepest slope −25‰
Decrease in marine export production	−8.6	−0.2	steeper slope with $y_0 = -9.7‰$ during first 50 years
Rise in NADW formation	−7.8	+0.6	varies with time; mixture with changes in marine export production during Heinrich 1 event; during Younger Dryas and resumption in the Holocene $y_0 = -7.15 \pm 0.05‰$, steep slope during first 50 y with $y_0 = -9.5‰$
Rise in Southern Ocean vertical mixing	−8.2	+0.2	steep slope during first 50 years with $y_0 = -11.0‰$
Decline in sea ice cover/rise in gas exchange rates	−0.7	+7.7	regression over whole data set finds −3.8‰ with differences in the North (−4.8‰) and the South (−77.2‰)
Rise in sea level	−6.4	+2.0	
Rise in temperature	−3.6	+4.8	
Sediment/ocean interaction	−5.8	+2.6	

556

Table 4. Regression analysis of time windows in the combined scenario A-TB2 covering carbon cycle dynamics during Termination I. Results in 100 years resolution.

#	Time (kyr BP)	y_0 (‰) r^2 (%) in brackets	Main processes
1	20.0–17.1	−7.3 (65)	Reduction in marine export production
2	17.0–16.9	−10.0 (100)	Increase in Southern Ocean mixing
3	16.8–16.6	−5.2 (97)	nothing special
4	16.5–14.9	−11.4 (83)	NADW and export production reduced in Heinrich event 1 and terrestrial carbon storage
5	14.8–14.3	−13.3 (90)	NADW rise in Bølling/Allerød and mainly terrestrial carbon storage
6	14.2–11.8	−13.0 (76)	NADW reduced in Younger Dryas and and terrestrial carbon storage
7	11.7–10.0	−6.9 (6)	nothing special, equilibration to interglacial climate

557
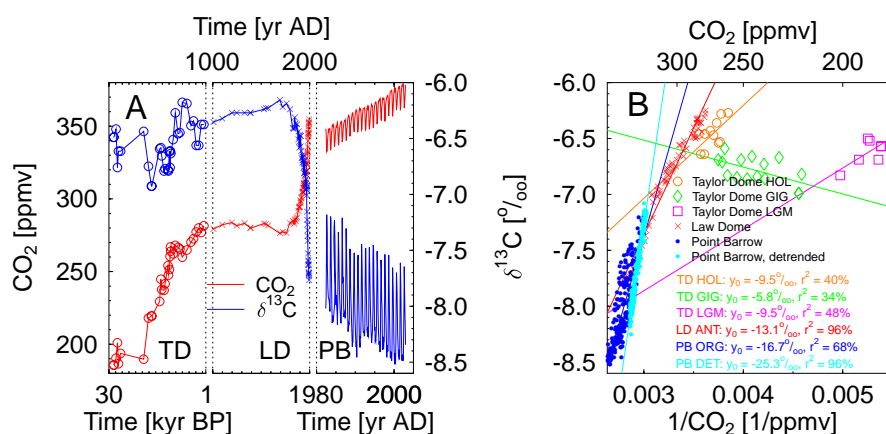
Fig. 1. A compilation of data from Point Barrow (PB), the Law Dome (LD), and the Taylor Dome (TD) ice cores (**A**: CO_2, δ^{13}C; **B**: Keeling plot). Monthly resolved data (1982–2002) from Point Barrow (Keeling and Whorf, 2005; Keeling et al., 2005). Only times where data in both CO_2 and δ^{13}C were available are considered here. For the Keeling plot approach the original data (PB ORG) and detrended time series (PB DET) are plotted and analysed. Data from firn and ice at Law Dome cover the last millenium (Francey et al., 1999; Trudinger et al., 1999) which includes the anthropogenic rise in CO_2 (LD ANT). Data from the Taylor Dome ice core of the last 30 kyr include the glacial/interglacial transition during Termination I (Smith et al., 1999) with the age model of Brook et al. (2000). Taylor Dome data are split into the Holocene (TD HOL), the glacial/interglacial transition (TD GIG), and the LGM (TD LGM).
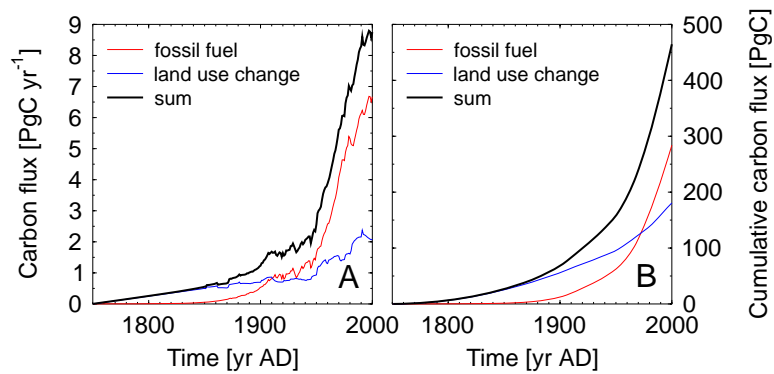
Fig. 2. Fossil fuel emissions since 1750 AD (Marland et al., 2005), land use change since 1850 AD (Houghton, 2003), linearly extrapolated to zero in year 1750 AD. **(A)** Annual fluxes; **(B)** Cumulative fluxes.

559
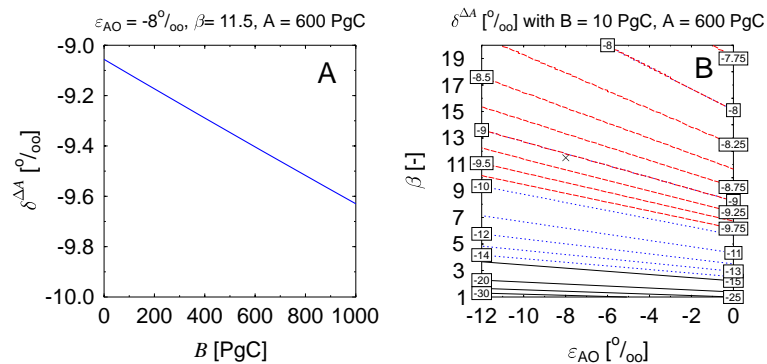
Fig. 3. Results of the extended Keeling approach with three reservoirs. Effective isotopic signature of the atmosphere $\delta^{\Delta A}$ as function of **(A)** the size of the terrestrial release and **(B)** the Revelle Factor β and the fractionation during gas exchange ε_{AO}. Other variable as given in the figures. The cross in panel (B) marks the preindustrial state (β=11.5, ε_{AO}=−8.0‰).
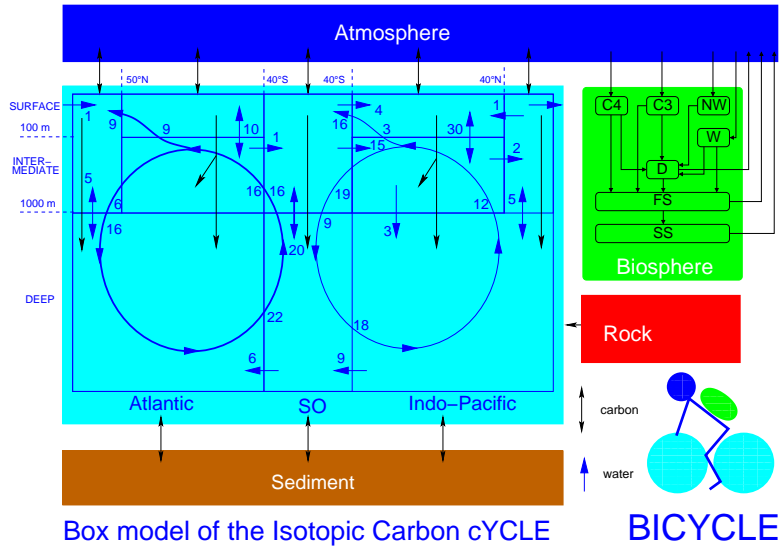
Fig. 4. A sketch of the BICYCLE model including boundary conditions and preindustrial ocean circulation fluxes (in Sv=10^6 m^2 s^{-1}) in the ocean module. The globally averaged terrestrial biosphere distinguishes ground vegetation following different photosynthetic pathways (C4, C3), non-woody (NW), and woody (W) parts of trees, and soil compartments (D, FS, SS) with different turnover times.

561
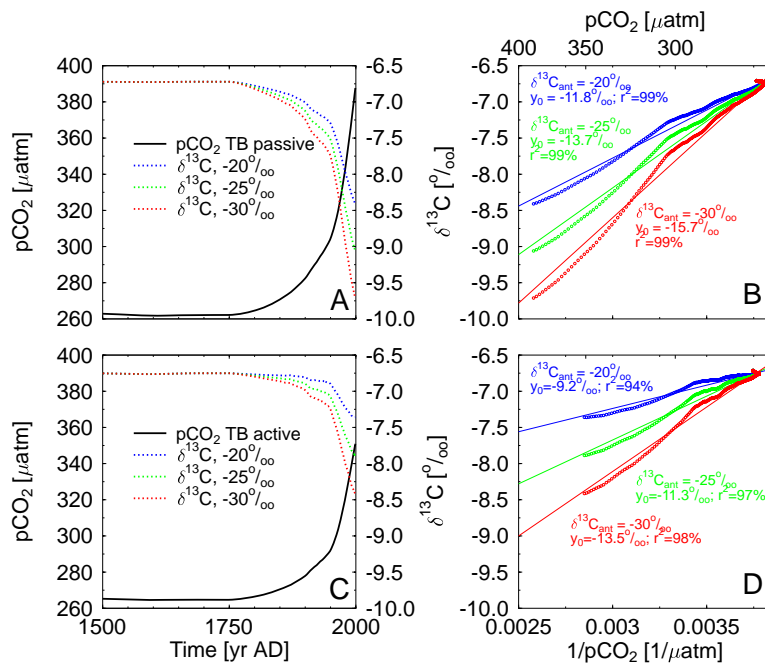
Fig. 5. Reconstructions of the rise in pCO$_2$ during the last 500 years with BICYCLE (left: pCO$_2$, δ^{13}C; right: Keeling plot). Anthropogenic fluxes were used as plotted in Fig. 2. Two different settings are tested, one with passive terrestrial biosphere TB (top), meaning that carbon storage in the land reservoirs was kept constant, and one with active terrestrial biosphere (bottom), in which a rise in the internal calculated pCO$_2$ is enhancing terrestrial carbon uptake via its fertilisation effect. Different simulations with different isotopic signatures of the anthropogenic emission (−20‰, −25‰, −30‰).

562
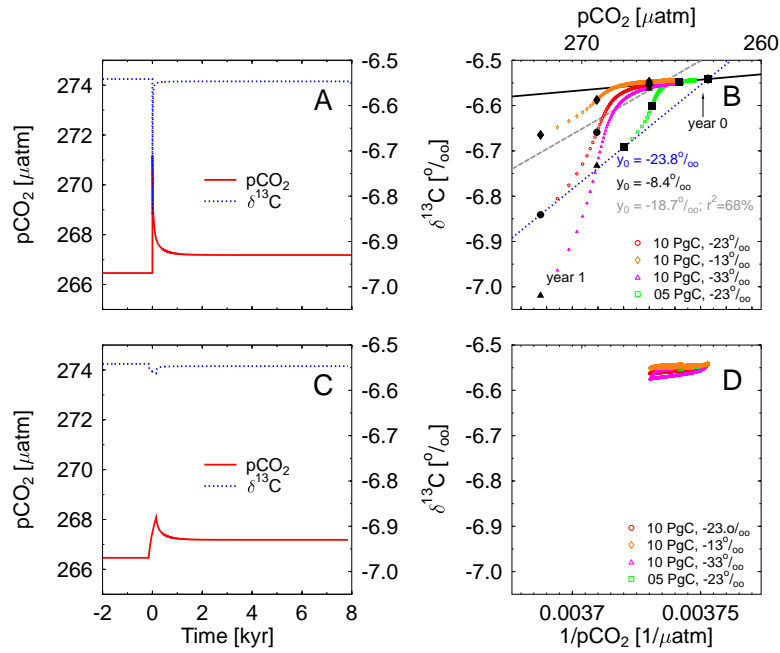
Fig. 6. Effect of a pulse of instantaneous release (within one year) of terrestrial carbon with an isotopic signature of $\delta^{13}C = -23\permil$ (left: pCO_2, $\delta^{13}C$; right: Keeling plot). Different carbon release amplitudes (5, 10 PgC) and different $\delta^{13}C$ signatures ($-13\permil$, $-23\permil$, $-33\permil$) are tested. The regression functions seen in **(B)** are for the three different regression models for the 10 PgC/$-23\permil$ scenario (red circles). Model 1: year 0 and year 1 (short dash); model 2: year 0 and year 8000 (solid); model 3: regression through 375 years (long dash). Large black markers mark the years 0, 1, 10, 100 in each record. Bottom: Same as above but now the data are smoothed with a 300 yr running mean.
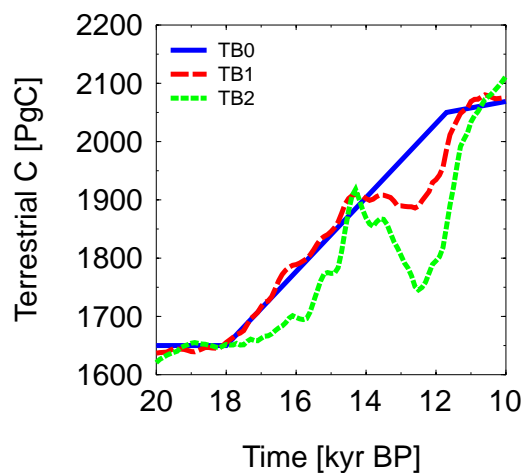
Fig. 7. Changes in the terrestrial carbon storage during the last glacial/interglacial transition follows a null-model of linear increase (TB0) or two different dependencies dominated by CO_2 fertilisation (TB1) or climate (TB2). Scenarios taken from Köhler et al. (2005a).
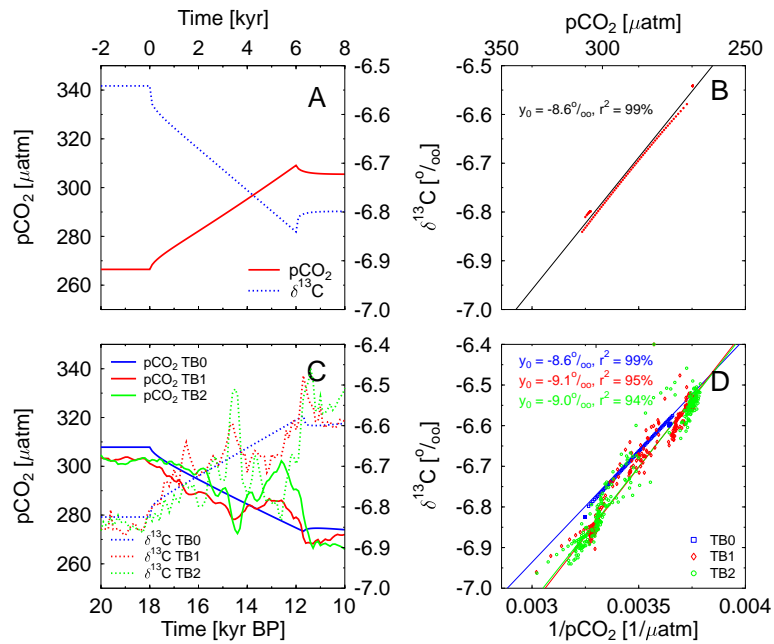
Fig. 8. Effects of a gradual change in the carbon storage of the terrestrial biosphere (left: pCO$_2$, δ^{13}C; right: Keeling plot). Top: Linear decrease in terrestrial carbon storage by 500 PgC. Bottom: Scenarios TB0 (biosphere only, linear increase in terresterial carbon by 400 PgC between 18 and 11.8 kyr BP) TB1 (dominated by CO$_2$ fertilisation) and TB2 (dominated by climate change) as shown in Fig. 7. Regressions in the Keeling plots are performed over the whole time period.
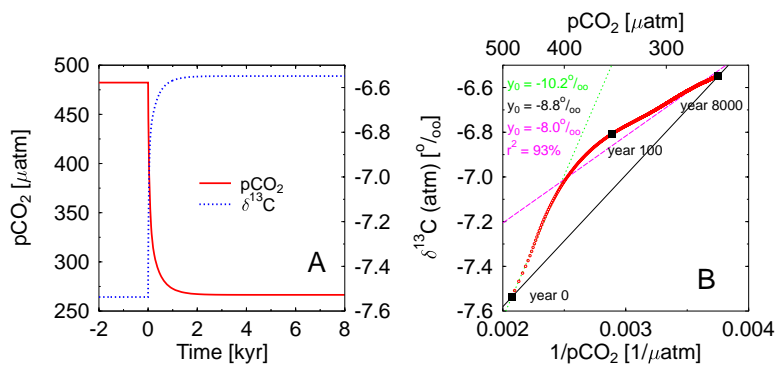
<center>565</center>

Fig. 9. Switching from an abiotic to a biotic ocean at t=0 kyr (**A**: pCO$_2$, δ^{13}C; **B**: Keeling plot). Different regression models in (B): model 1 (first year only) in green; model 2 (prior/after) in black; model 3 (equilibration time) in magenta.

<center>566</center>
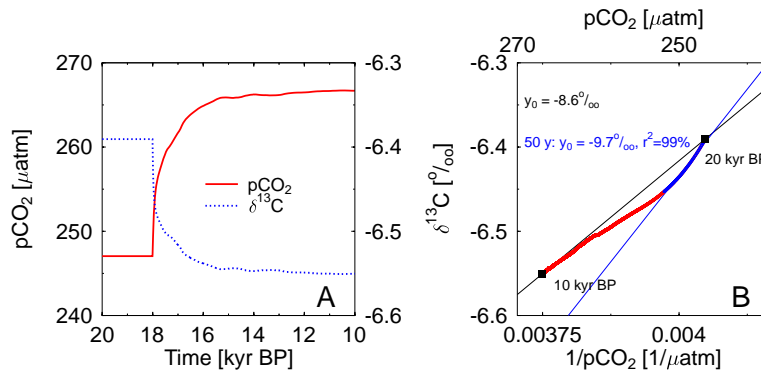
Fig. 10. Effects of iron fertilisation in the Southern Ocean on atmospheric carbon records with scenario taken from Köhler et al. (2005a) (**A**: pCO_2, $\delta^{13}C$; **B**: Keeling plot). Blue dots and regression in (B) over the first 50 years during pCO_2 rise only.
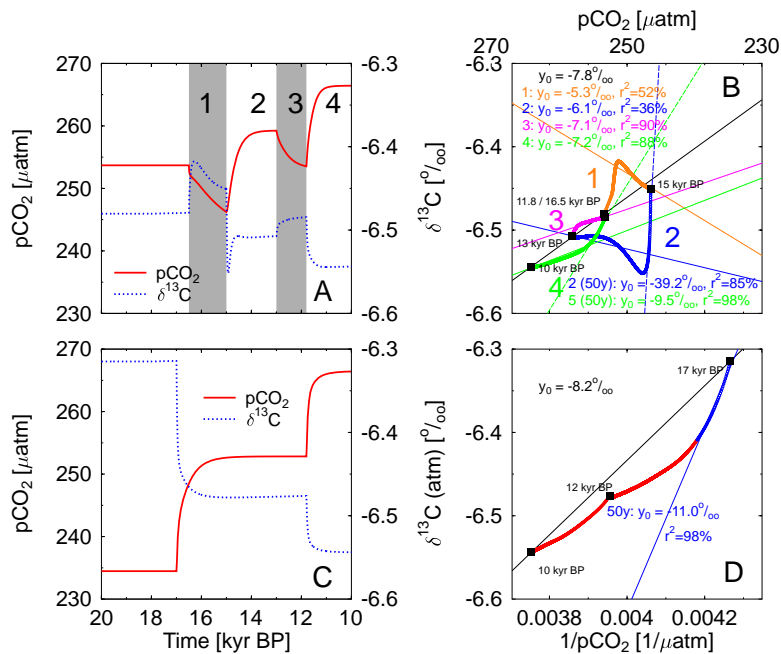
567

Fig. 11. Simulated effects of changes in the strength of the NADW formation (top) and Southern Ocean vertical mixing (bottom) as used in Köhler et al. (2005a) (left: pCO_2, $\delta^{13}C$; right: Keeling plot). Four different time intervals with different strength in NADW formation are identified and labeled in **(A)** and **(B)**. Regression are performed for the prior/after situation (black, B, D), for these four time intervals (B) and for selected 50 year time windows (B, D).
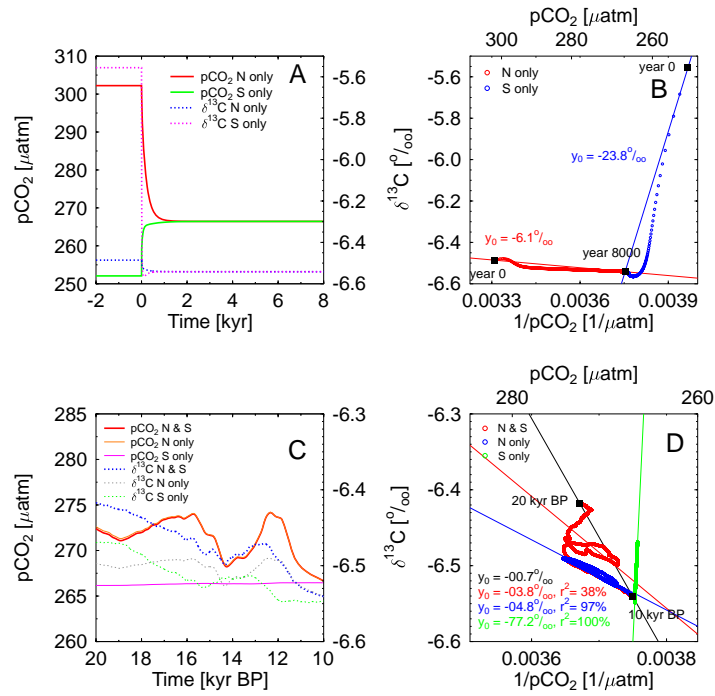
Fig. 12. Simulated effects of an instantaneous change in sea ice cover from total coverage to preindustrial values in the North Atlantic (top: N only), or the Southern Ocean (top: S only) and as in the scenario used in Köhler et al. (2005a) (left: pCO_2, $\delta^{13}C$; right: Keeling plot). In the Termination I scenario (bottom) the contribution of northern (N only) and southern (S only) sea ice is shown individually and in a combined scenario (N & S). Regressions for the prior/after situation are shown everywhere, in D regressions over the whole period are shown additionally.

569
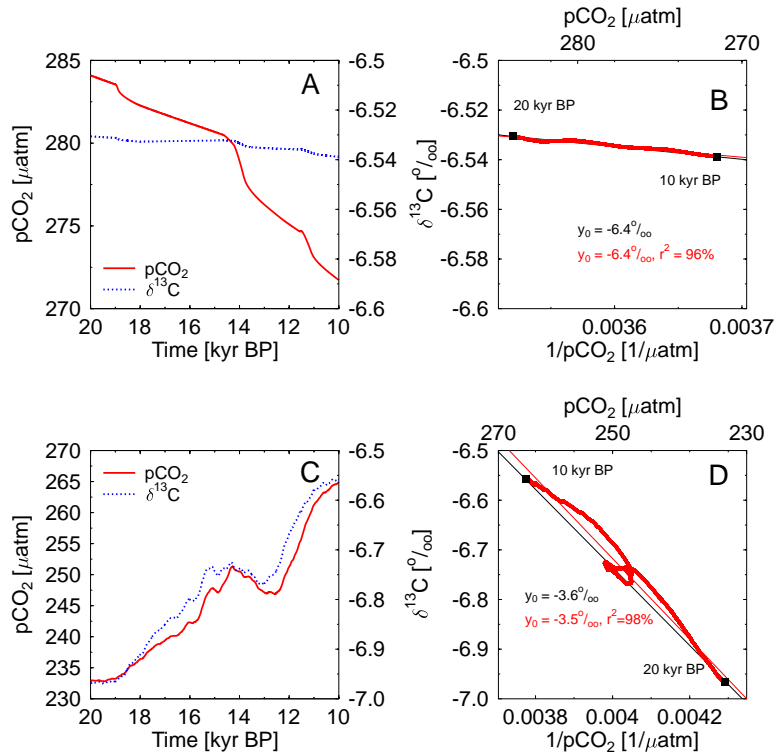
Fig. 13. Simulated effects of sea level rise (top) and ocean temperature change (bottom) as used in Köhler et al. (2005a) (left: pCO_2, $\delta^{13}C$; right: Keeling plot). Regression of the prior/after analysis (black) and over the whole period (red) are shown.
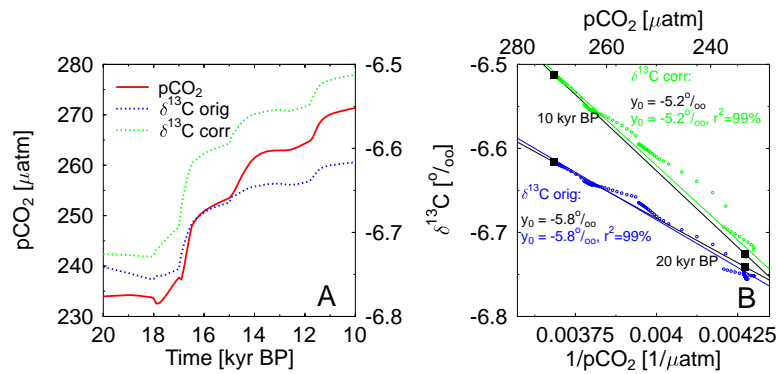
570

Fig. 14. Estimation of the effect of sediment/ocean fluxes of $CaCO_3$ on the atmospheric carbon records by subtracting the results of a scenario with all processes but the $CaCO_3$ effect in operation from the combined scenario. Terrestrial biosphere is following a linear glacial/interglacial rise (TB0 in Fig. 7). **(A)**: pCO_2 and $\delta^{13}C$. **(B)**: Keeling plot. Regression of the prior/after analysis (black) and over the whole period (blue, green) are shown. The original $\delta^{13}C$ (orig) and $\delta^{13}C$ corrected (corr) for the trend in the mean $\delta^{13}C$ caused by the sedimentation losses are shown.
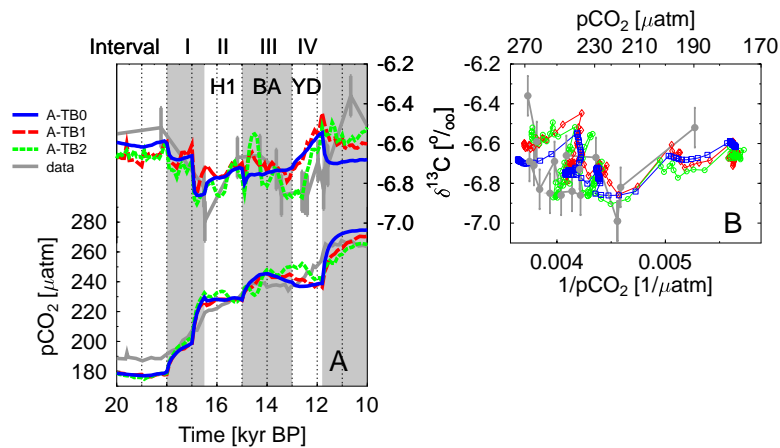
Fig. 15. **(A)**: Measured and simulated atmospheric carbon records over Termination I: Data: Atmospheric $\delta^{13}C$ in the Taylor Dome ice core (Smith et al., 1999); pCO_2 in the EPICA Dome C ice core divided in four intervals with different changing rates (Monnin et al., 2001). Both data set are synchronized to the GISP2 age scale (Meese et al., 1997). The intervals II, III, and IV are approximately identical with the Heinrich 1 event (H1), the Bølling-Allerød warm interval (BA), and the Younger Dryas cold event (YD) in the North Atlantic region. Simulation scenarios combine all physical processes (ocean temperature, sea level, sea ice) with changes in ocean circulation (NADW formation, Southern Ocean mixing), marine export production, $CaCO_3$ compensation and terrestrial biosphere. Differences in the scenarios A-TB0, A-TB1, and A-TB2 are the simulated changes the terrestrial carbon storage, which are shown in Fig. 7. **(B)**: Keeling plot. Note, that the measured CO_2 data are given in volume mixing ratio (ppmv), while the model calculates the partial pressure (pCO_2) in units of μatm.
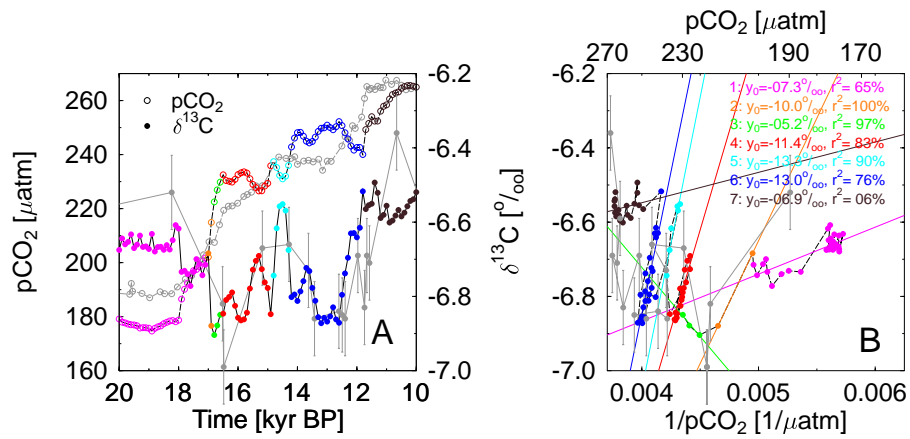
Fig. 16. A detailed look at scenario A-TB2 (colors) in comparision to the Taylor Dome δ^{13}C and EPCIA Dome C CO_2 data (grey) during Termination I (10–20 kyr BP). **(A)**: pCO$_2$ (open circles), δ^{13}C (closed circles); **(B)**: Keeling plot. Seven time windows showing different dynamics and their regression functions are marked with different colors. Note, that the measured CO_2 data are given in volume mixing ratio [ppmv], while the model calculates the partial pressure (pCO$_2$) in units of μatm.

573